applied sciences

MDPI

Article

Quantifying Impact Damage Severity in Conventional, Hybrid and Natural-Based Composite Structures: An Acousto–Ultrasonics Approach

Kumar Shantanu Prasad [1,*], Gbanaibolou Jombo [1,*], Sikiru O. Ismail [1], Yong K. Chen [1] and Hom Nath Dhakal [2]

[1] Centre for Engineering Research, School of Physics, Engineering and Computer Science, University of Hertfordshire, Hatfield AL10 9AB, UK; s.ismail3@herts.ac.uk (S.O.I.); y.k.chen@herts.ac.uk (Y.K.C.)

[2] Portsmouth Centre for Advanced Materials and Manufacturing (PCAMM), School of Electrical and Mechanical Engineering, University of Portsmouth, Portsmouth PO1 3DJ, UK; hom.dhakal@port.ac.uk

* Correspondence: kumarshantanu1996@gmail.com (K.S.P.); g.jombo@herts.ac.uk (G.J.)

Abstract

This study presents an approach to quantifying impact-induced damage severity in composites, focusing on synthetic carbon fibre-reinforced polymer (CFRP), natural flax fibre-reinforced polymer (FFRP) and hybrid fibre reinforced polymer (HFRP) composite of carbon and flax. The investigation aims to quantitatively characterise impact damage under energies ranging from 10 to 70 J through acousto–ultrasonics (AU) testing, proposing an efficient technique for evaluating the integrity of various FRP composites under in-service conditions. AU testing was performed at azimuthal angles of 0°, 30°, 45°, 60° and 90°, utilising acousto–ultrasonic waveform indices (AUWIs), such as wave velocity, peak amplitude, energy content, centroid frequency and skewness factor. The damage severity index is correlated with the damage mode. The findings establish that wave velocity is a reliable parameter for quantifying damage severity across all composite material types considered, with high adjusted R^2 values of 0.92 for CFRP, 0.89 for FFRP and 0.90 for HFRP. Peak amplitude also shows considerable sensitivity. Finally, this research highlights the limitations of traditional non-destructive evaluation (NDE) techniques and demonstrates the potential of combining multi-damage metrics with advanced imaging methods, such as X-ray micro-computed tomography (X-ray μCT) and scanning electron microscopy (SEM), to provide a comprehensive assessment of damage in various composite materials. The proposed methodology offers a promising approach for quantifying the impact damage severity in composite structures, as applicable to wind turbine blades, amongst other structural components.

Keywords: acousto–ultrasonics; structural health monitoring; damage severity; non-destructive evaluation; stress-wave factor

Academic Editor: Michel Darmon

Received: 24 April 2026
Revised: 9 June 2026
Accepted: 10 June 2026
Published: 23 June 2026

1. Introduction

The growing utilisation of composite materials, particularly in high-performance applications such as wind turbine blades and the aerospace and automotive industries, necessitates the use of advanced structural health monitoring (SHM) techniques to ensure the integrity and safety of these structures. Carbon fibre-reinforced polymers (CFRPs),

flax fibre-reinforced polymers (FFRPs), and hybrid fibre-reinforced polymers (HFRPs) represent a spectrum of composites that combine synthetic and natural fibres to balance mechanical properties and environmental/sustainability impact. However, these materials are susceptible to damage modes under impact loading. These damage responses include, but are not limited to, matrix cracking, delamination and fibre breakage. They critically compromise the structural performance of composites under operational loads.

Carbon fibre-based polymer systems are also increasingly used in civil and industrial structures, where carbon fibre fabric/sheet-based strengthening systems are externally bonded to concrete, steel, timber or masonry members to improve stiffness, load-carrying capacity, fatigue resistance and serviceability performance [1]. Recent work on machine-induced vibrations in industrial building floors has further demonstrated the importance of experimental and numerical assessment of carbon-fibre-based polymer systems under operational dynamic excitation [2]. These systems share with CFRP laminates the dependence on carbon-fibre stiffness, polymer–matrix load transfer, interfacial integrity and vibration-sensitive response. However, their structural function differs from the standalone CFRP laminates considered in the present study: CFFS-based systems are usually bonded to larger civil infrastructure components and are evaluated at the global structural scale, whereas the present CFRP, FFRP and HFRP laminates are evaluated as composite plates subjected to localised impact damage and interrogated through acousto–ultrasonic wave propagation.

Conventional non-destructive evaluation techniques used for fibre-reinforced polymer composites include pulse-echo and through-transmission ultrasonics, phased-array ultrasonics, acoustic emission, infrared thermography, shearography, radiography and X-ray computed tomography. Ultrasonic inspection is extensively used for detecting internal discontinuities, delamination, voids and impact-induced damage in composite structures. However, its performance may be influenced by fibre-induced anisotropy, high attenuation, coupling conditions, component geometry and defect orientation. Recent advances in ultrasonic modelling and imaging have expanded the application of conventional bulk-wave, guided-wave and phased-array techniques for the inspection and structural health monitoring of complex composite structures [3].

X-ray-based techniques provide complementary information on the internal structure and damage state of FRP composites. Conventional radiography produces two-dimensional projections, whereas X-ray micro-computed tomography enables non-destructive three-dimensional visualisation of fibre architecture, manufacturing defects, voids, matrix cracking, delamination and internal damage progression. Advanced phase-contrast X-ray imaging can further separate attenuation, phase and scattering information, thereby improving the characterisation of carbon composites with low conventional absorption contrast [4–6]. Scanning electron microscopy is also widely used as a complementary post-damage characterisation technique because it provides high-resolution observations of fracture surfaces and local damage mechanisms, including matrix cracking, fibre pull-out, fibre breakage and fibre–matrix debonding [7]. However, SEM is generally localised and may require specimen preparation; consequently, it is more suitable for validating microscopic failure mechanisms than for in-service volumetric inspection.

Although these methods provide valuable damage information, each technique has different spatial resolution, penetration depth, inspection area and operational limitations. Therefore, the combination of stress-wave-based monitoring with complementary X-ray μCT and SEM observations can provide a more comprehensive assessment of damage in FRP composites. In the present study, AUT is used as the primary quantitative damage severity technique, while X-ray μCT and SEM are employed to independently validate the corresponding internal and microscopic damage mechanisms [8,9].

Acousto–ultrasonic waveform indices (AUWIs), including peak amplitude, wave velocity, energy content, centroid frequency and skewness factor, serve as quantitative indicators of damage severity in composites. Previous research has demonstrated empirical correlations between AUWIs or Guided Lamb-wave utilisation and damage levels [10–17]. However, these studies do not fully establish a unified framework linking multiple AUWIs to specific impact-induced damage mechanisms across synthetic, natural, and hybrid fibre-reinforced composites tested over several azimuthal angles. Moreover, the complex interplay between different fibres in hybrid composites adds another layer of challenge, as these materials exhibit unique attenuation and dispersion characteristics that are not adequately addressed by current models.

Unlike previous studies, which focused on AUT damage severity on light-to-moderately attenuative composite material, such as CFRP composite materials, the novelty of this study lies in examining AUT's capabilities for damage severity characterisation on moderate-to-highly attenuative composite material, including both hybrid and natural FRP materials (especially flax and hemp) across multiple azimuthal angles and impact energies. By employing several AUWIs quantitative metrics, this paper bridges the research gap between qualitative detection and quantitative characterisation for impact damage, providing a robust methodology for assessing the integrity of composite materials under in-service conditions.

Furthermore, by integrating the damage severity indices with regression models, this study demonstrates a predictive capability, using AUT for damage progression estimation in composites with experimental validation.

The novelty of the present study lies in the development of a comparative acousto–ultrasonic damage severity framework for synthetic, natural and hybrid fibre-reinforced polymer composites subjected to controlled impact loading. Previous AU, Lamb-wave-based and conventional NDE studies have mainly focused on damage detection, delamination identification or qualitative assessment of damage in conventional CFRP-type laminates. In contrast, the present work extends the application of the AUT towards quantitative impact damage characterisation by evaluating multiple acousto–ultrasonic waveform indices across CFRP, FFRP and carbon/flax HFRP composite laminates.

The specific contribution of this study is that the AU response is examined across five impact energy levels, namely 10, 20, 30, 50 and 70 J, and five azimuthal angles, namely 0°, 30°, 45°, 60° and 90°. This allows the influence of material type, fibre architecture, propagation direction and damage severity to be assessed systematically. Furthermore, the study does not rely solely on waveform variation, but correlates AU waveform indices with independently observed damage mechanisms using X-ray micro-computed tomography and scanning electron microscopy. This provides a stronger physical basis for linking changes in wave velocity, peak amplitude, energy content, centroid frequency and skewness factor with matrix cracking, delamination, fibre pull-out and fibre breakage.

Therefore, the present study differs from earlier AU and Lamb-wave investigations by moving beyond qualitative detection towards quantitative damage severity evaluation in composite systems with different attenuation and damping characteristics. This is particularly important for natural and hybrid FRP composites, where the higher damping capacity and heterogeneous fibre–matrix architecture can significantly affect stress-wave propagation. The proposed approach therefore provides a more comprehensive basis for applying AUT to the structural health monitoring of advanced composite structures, including wind turbine blade composites, aerospace components and other impact-sensitive engineering structures.

2. Materials and Methods

2.1. Materials

The study utilised three types of composite laminates:

- Carbon fibre-reinforced polymer (CFRP): Representing synthetic fibre material known for its high stiffness and strength-to-weight ratio.
- Flax fibre-reinforced polymer (FFRP): Indicating sustainable composites with notable high damping property and high attenuation.
- Carbon/flax hybrid fibre reinforced polymer (HFRP): Combining the advantages of synthetic and natural fibres to leverage hybridisation concept.

These materials were chosen to explore the effects of different fibre types and material attenuation effect on damage detection and severity quantification, using AUT.

The CFRP, FFRP and HFRP composite plates, of dimension 250 mm × 250 mm × 4 mm each, were fabricated with the intention to provide some tolerance for cutting. The composite laminates were manufactured using the resin infusion technique. The flax fibre fabrics were dried thoroughly in the oven at 60 °C for about 15 min before usage. The product was vacuum sealed at a pressure of 0.88 bar and at room temperature.

Easy composites EL2 epoxy resin was used for the manufacturing procedure, and it was combined with the AT30 slow hardener in a 1:4 ratio. The laminates were trimmed to the desired shape and size. All the fabricated laminates had a thickness equal to 4 ± 0.2 mm. Each carbon and flax sheet is between 0.20 and 0.22 mm thick. Table 1 presents the summarised data of the materials used. All the samples were unidirectional.

Table 1. Material properties of CFRP and FFRP.

Material Properties	Carbon/Epoxy (CFRP)	Flax/Epoxy (FFRP)
Number of layers (for 4 mm thick plate)	20	20
Density (kg/m^3)	1550	1400
E_{11} (Pa)	1277×10^8	800×10^8
E_{22} (Pa)	74×10^8	30×10^8
E_{33} (Pa)	74×10^8	30×10^8
G_{12} (Pa)	69×10^8	20×10^8
G_{13} (Pa)	69×10^8	20×10^8
G_{23} (Pa)	43×10^8	10×10^8
ν_{12}	0.3286	0.3530
ν_{13}	0.3316	0.3530
ν_{23}	0.1880	0.0670

2.2. Experimental Setup

2.2.1. Impact Testing

The tests were performed using an Instron CEAST 9340 (Figure 1), a high-precision drop-weight impact testing machine known for its reliability and advanced technical specifications. The apparatus was equipped with a hemispherical impactor constructed from steel, measuring 20 mm in diameter. The impacting mass used was 5 kg. The sample dimensions were 220 mm × 220 mm × 4 mm, adhering to ASTM D2344 [18] standards.

The incident energy levels were kept constant during testing, while other parameters, such as impact velocity and drop height, were adjusted to achieve the desired energy levels. The impact testing involved five distinct levels of incident energies of 10, 20, 30, 50 and 70 J at impact velocities of 1.567, 2.215, 2.713, 2.927 and 3.391 m/s, respectively. The variations in energy were intended to demonstrate different levels of impact damage severity, which induced various types of damage modes within the composite laminates.

This approach helps in understanding the performance of the materials under varied impact conditions.

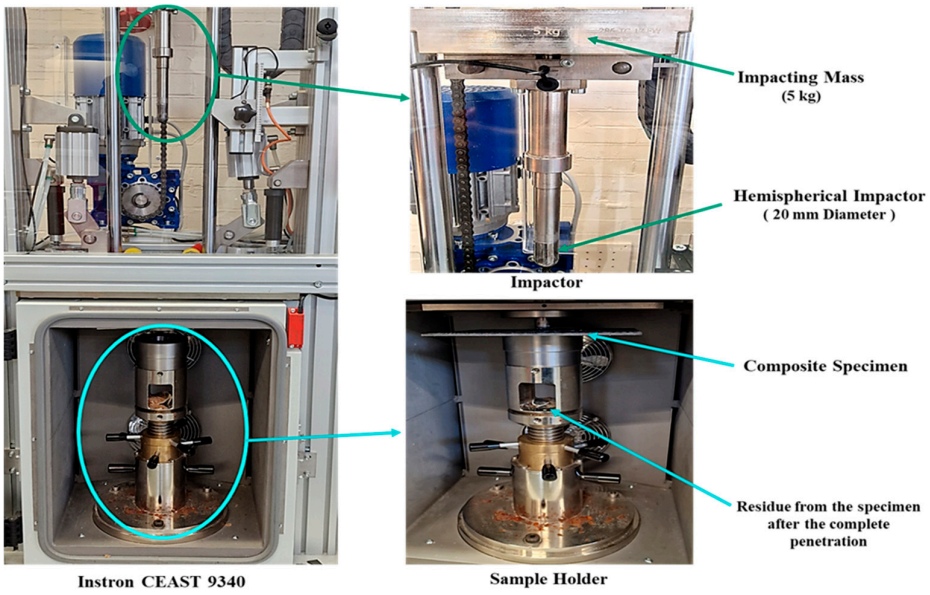

Figure 1. Impact testing to induce different damage modes.

For each composite material type and impact energy level, separate specimens were used rather than applying successive impacts to the same specimen. Therefore, the damage states generated at 10 J, 20 J, 30 J, 50 J and 70 J represent discrete impact conditions rather than cumulative damage progression on a single laminate. This approach was adopted to avoid the interaction of previous damage with subsequent impact events and to allow each impact energy level to be interpreted independently. For each material and impact energy condition, three specimens were tested to improve repeatability and to account for specimen-to-specimen variability.

2.2.2. Acousto–Ultrasonics Testing

Acousto–ultrasonics (AU) is an active stress-wave-based NDE technique in which a controlled ultrasonic excitation is introduced into a material using a piezoelectric transmitter, while the propagated response is recorded at a second location by a receiver [19,20]. Unlike passive acoustic emission methods, which depend on the spontaneous release of elastic energy from an actively growing defect, AUT interacts with the structure using an externally imposed and repeatable input signal. This enables the material state to be examined in a controlled manner and makes AUT particularly suitable for composite laminates, where damage is often subsurface, spatially distributed, and not readily identifiable through surface inspection alone [21,22]. The method is therefore well suited to structural integrity assessment in FRP composites subjected to impact loading. The operating mechanism of AUT may be described in four successive stages: wave generation, wave propagation, wave interaction with internal defects and signal interpretation. Once introduced into the laminate, the guided stress wave travels through the material and interacts with its anisotropic architecture, including fibre alignment [23], interfaces between constituents, and any impact-induced damage present within the propagation path. Defects, such as matrix cracking, delamination, fibre breakage and fibre–matrix debonding alter the transmitted response through attenuation, scattering, reflection, mode conversion and local changes in propagation velocity [15,19]. Consequently, the received AUT waveform contains integrated information about the condition of the material volume

located between the transmitting and receiving sensors, rather than information from a single localised point only. This volumetric sensitivity is one of the key advantages of AUT for the damage assessment of laminated composite structures. This characteristic is especially important for impact-damaged composite structures, where the damage state is generally multi-mechanistic and evolves progressively with increasing impact severity. In conventional synthetic laminates, such as CFRP, as well as natural-based and hybrid laminates, including FFRP and carbon/flax composites, impact can induce combinations of matrix cracking, delamination, fibre failure and interfacial damage. Since these damage modes influence the stiffness, continuity and damping behaviour of the laminate, they also influence stress-wave propagation. For this reason, AUT offers a practical route not only for detecting the presence of damage, but also for quantifying its severity through measurable changes in waveform features [20,24].

In the present work, the AUT response was analysed using a set of AUWIs extracted from both the time and frequency domains, namely peak amplitude, wave velocity, energy content, centroid frequency, and skewness factor. These indices were selected because they represent complementary descriptors of wave– material interaction. Peak amplitude reflects signal attenuation associated with damage progression; wave velocity is related to the effective stiffness of the propagation path and is highly sensitive to internal degradation; energy content represents the overall transmitted wave energy; centroid frequency reflects redistribution of spectral content; and skewness factor provides additional information concerning the asymmetry of the frequency distribution and the heterogeneous nature of the damaged medium. By correlating these AUWIs with increasing impact energy and with damage modes validated independently using micro-CT and SEM, the methodology provides a quantitative basis for evaluating damage severity rather than only identifying damage occurrence [24,25].

AUT signals were generated using a broadband pulse generator and received with a piezoelectric transducer. The transducer was aligned to capture signals at the specified azimuthal angles, with data acquisition performed using an oscilloscope and subsequent FFT analysis.

Figure 2 shows the experimental setup adopted for the AUT investigation. The wave velocities and other AUWIs were determined from the acquired waveforms, and the measurements were conducted at selected azimuthal angles to account for the anisotropic nature of the investigated composite laminates. This approach enabled the influence of both material type and propagation direction on impact damage sensitivity to be systematically evaluated. An ultrasonic piezoelectric transducer of 1 MHz and a resonant-type AE transducer with a resonant frequency of 150 MHz was employed as a transmitter and a receiver, respectively. The sensors were attached to the plate using beeswax, acting as a couplant. Across the procedure, an effective contact pressure of 0.060 MPa was used between the sensor and the testing plate. To drive and send the signal to the ultrasonic transducer, an arbitrary function generator was introduced to produce a 3-cycle sine wave tone burst manual signal with a peak-to-peak amplitude of 15.8 mV. This signal was then fed to an RF power amplifier of 50 dB to boost/amplify the sending wave to a peak-to-peak amplitude of 5 V. Moreover, on the receiver's end, the narrow band resonant-type AE sensor, which has a flat frequency response up to 750 kHz, with a resonant peak at 150 kHz, was connected to the AE signal acquisition system configured with a measuring rate of 5 MHz. Additionally, analogue and digital Butterworth bandpass filters covering frequencies from 20 to 1000 kHz and 80 to 100 kHz, respectively, were configured to avoid the insertion of ambient noise into the AU-acquired signal.

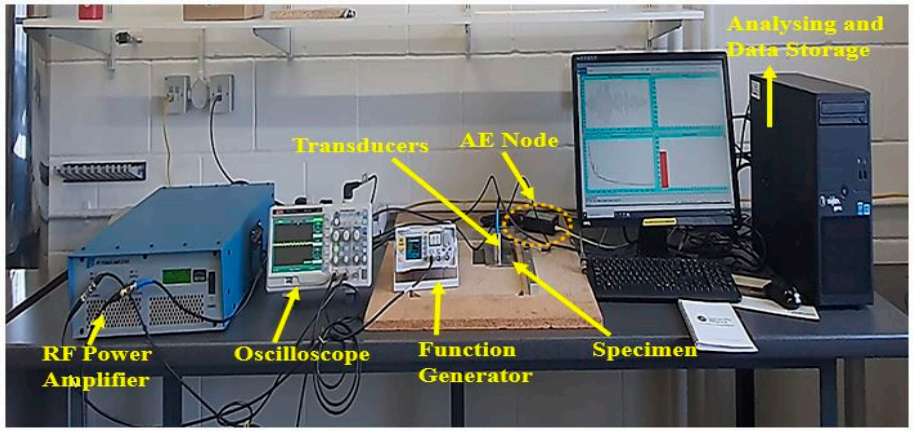

Figure 2. AU testing setup.

Experimentally, the phase velocity of the wave propagation was obtained by using the method proposed by Kiernan [26], governed by Equation (1).

$$V_{ph} = \Delta d/\Delta t \quad (1)$$

where V_{ph}, Δd and Δt represent the phase velocity (mm/s), difference in the sensor spacings (mm) and time difference (s), respectively. The Δt was calculated by tracing the same phase point on the waveform, showing the output for both sensor spacing at 60 and 120 mm. While Δd was determined by measuring the displacement of the sensor spacing, which was obtained as 60 mm.

Due to sample symmetry, the experiment was conducted at five distinct azimuthal angles of 0°, 30°, 45°, 60° and 90° across all FRP composite samples, namely CFRP, FFRP and HFRP composite samples. The testing procedure was carried out in two phases: before and after the impact events, allowing for a comparative assessment of the impact-induced damage. The schematic representation of the testing configuration is shown in Figures 2 and 3, providing a detailed overview of the setup and methodology employed in this study.

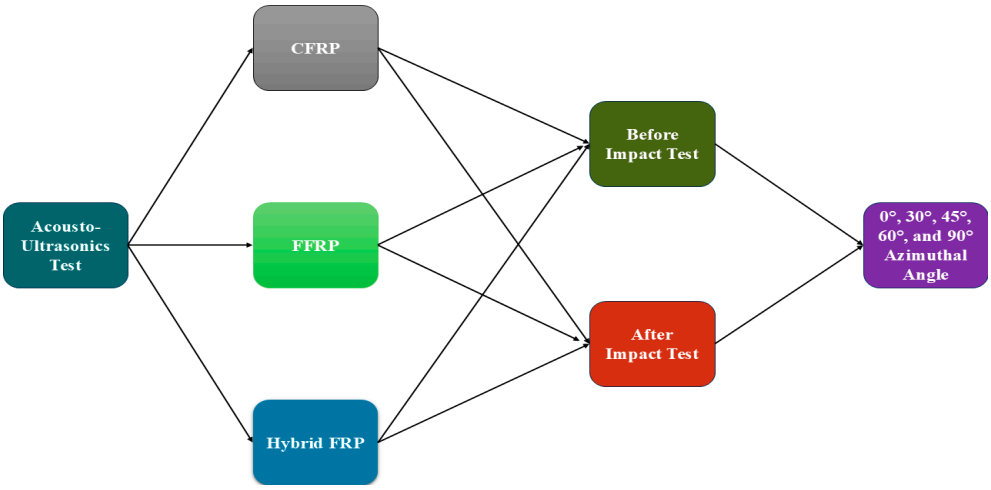

Figure 3. Schematic of testing modes in the polymer composites.

Experimental Repeatability and Measurement Uncertainty

To improve the repeatability of the acousto–ultrasonic measurements, each test condition was examined using a consistent sensor arrangement, excitation signal, sensor

spacing, contact pressure and coupling procedure. For each composite material type, namely CFRP, FFRP and HFRP, specimens were tested under five impact energy levels of 10, 20, 30, 50 and 70 J, in addition to the undamaged baseline condition. The AUT measurements were performed at five azimuthal angles of 0°, 30°, 45°, 60° and 90° before and after impact loading.

For each material type and impact energy level, three specimens were tested, and each AUT acquisition was repeated five times under the same experimental conditions. These repeated acquisitions were used to confirm waveform consistency and to minimise uncertainty associated with sensor coupling, contact pressure, signal acquisition and time-of-arrival identification. The mean waveform response was then used to extract the acousto–ultrasonic waveform indices for subsequent analysis.

The principal sources of uncertainty were associated with the repeatability of the couplant layer, contact pressure between the transducer and specimen, identification of the same phase point in the received waveform and local heterogeneity of the impact-damaged composite region. To reduce these effects, the same sensor spacing, couplant material, contact pressure and acquisition settings were maintained throughout the experimental programme. Where repeated data were available, the standard deviation was calculated to assess the variability of the extracted acousto–ultrasonic waveform indices.

To correlate the AUT damage severity indices to varied impact-induced damage modes, X-ray micro-computed tomography (X-ray μCT) and scanning electron microscopy (SEM) scans were taken to reveal the internal damage modes after each impact level for all three composite material types.

According to Kiernan and Duke [26,27], the azimuthal angle is the angular measurement that is related to a selected reference direction. In composite materials, the azimuthal angle (β) is normally aligned with the 0° fibre orientation, as depicted in Figure 4. This angle is very important in the study of wave propagation and the behaviour of materials, particularly in anisotropic composites, where parameters such as stiffness and wave speed can change dramatically, depending on the direction in which the wave is travelling.

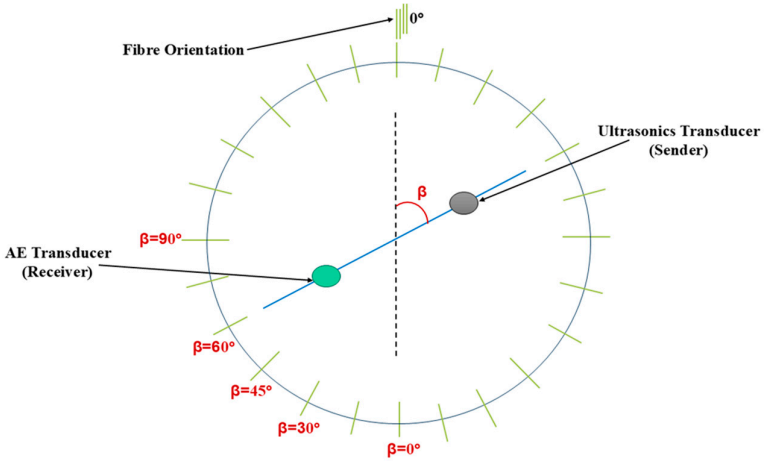

Figure 4. Definition of Azimuthal angle in polymer composites.

2.3. Data Analysis

AUT signals were analysed in both time and frequency domains. Key parameters (AUWIs) were extracted, as per [28,29]:

- Peak amplitude (AUWI1): Indicates the maximum signal strength, correlated with the extent of damage.

- Wave velocity (AUWI2): Derived from the time of arrival, reflecting changes in material stiffness due to damage.
- Energy content (AUWI3): Calculated as the area under the power spectral density curve, representing the overall energy of the AUT signal.
- Centroid frequency (AUWI4): The frequency at which the signal's energy is concentrated.
- Skewness factor (AUWI5): Measured asymmetry in the frequency distribution, associated with material anisotropy and heterogeneity.

Five acousto–ultrasonic waveform indices were extracted from the acquired signals, namely peak amplitude, wave velocity, energy content, centroid frequency and skewness factor. Peak amplitude was obtained from the maximum absolute amplitude of the received waveform. Wave velocity was calculated from the measured propagation distance and the time difference obtained by tracing the same phase point on the received waveform. Energy content was calculated from the area under the power spectral density curve. Centroid frequency was determined as the energy-weighted mean frequency of the received signal, while the skewness factor was used to describe the asymmetry of the frequency distribution.

To evaluate the relationship between AU waveform indices and impact damage severity, each AUWI was normalised with respect to its corresponding undamaged baseline value. The normalised AUWI values were then plotted against impact energy. A linear regression model was used to assess the relationship between each AUWI and impact energy for each material type and azimuthal angle [30,31]. The model used in this study is expressed as:

$$Y = aE + b$$

where Y is the normalised acousto–ultrasonic waveform index, E is the impact energy, and a and b are the regression coefficients. The adjusted coefficient of determination, adjusted R^2, was used to evaluate the strength of the linear relationship while accounting for the number of predictors in the model.

The linear regression model was selected because the objective of the analysis was to compare the relative sensitivity and consistency of the AUWIs across material type, impact severity and propagation direction, rather than to develop a complex predictive model. AUWIs with higher adjusted R^2 values were interpreted as having stronger linear association with increasing impact energy. However, indices with lower adjusted R^2 values were not discarded, as they may still provide complementary information related to attenuation, dispersion, frequency redistribution and anisotropic damage response [32,33].

3. Results and Discussions

3.1. AU Wave Analysis

Figures 5–9 show the AU output waveforms for CFRP at azimuthal angles of 0°, 30°, 45°, 60° and 90°, respectively. All Figures 5a–9a depict the signal for the undamaged sample, while Figures 5b–f–9b–f show the signals corresponding to impact energies of 10, 20, 30, 50 and 70 J, respectively.

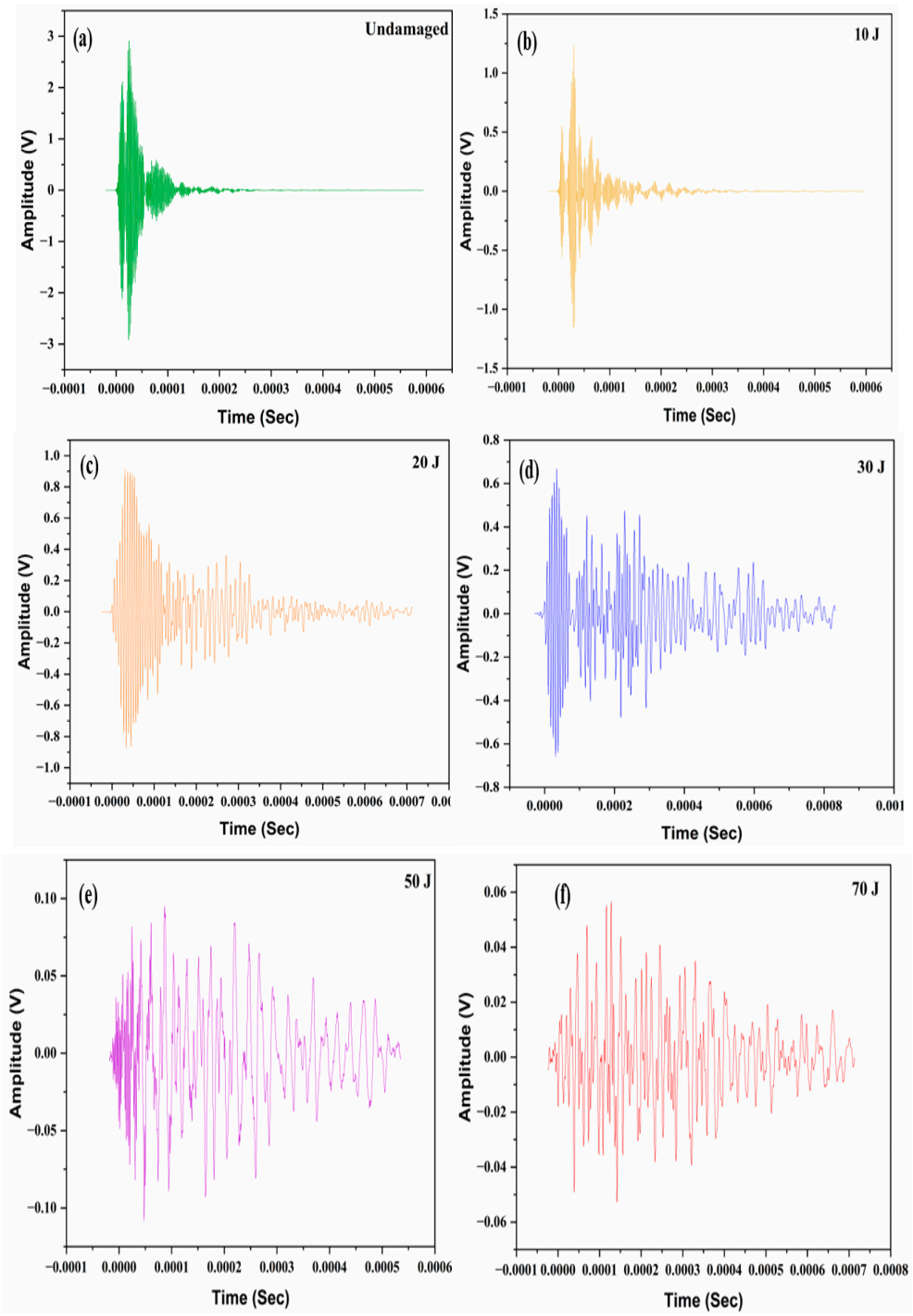

Figure 5. AU waveform for CFRP investigated at 0° for (**a**) Undamaged sample; (**b**) 10 J impacted sample; (**c**) 20 J impacted sample (**d**) 30 J impacted sample; (**e**) 50 J impacted sample; (**f**) 70 J impacted sample.

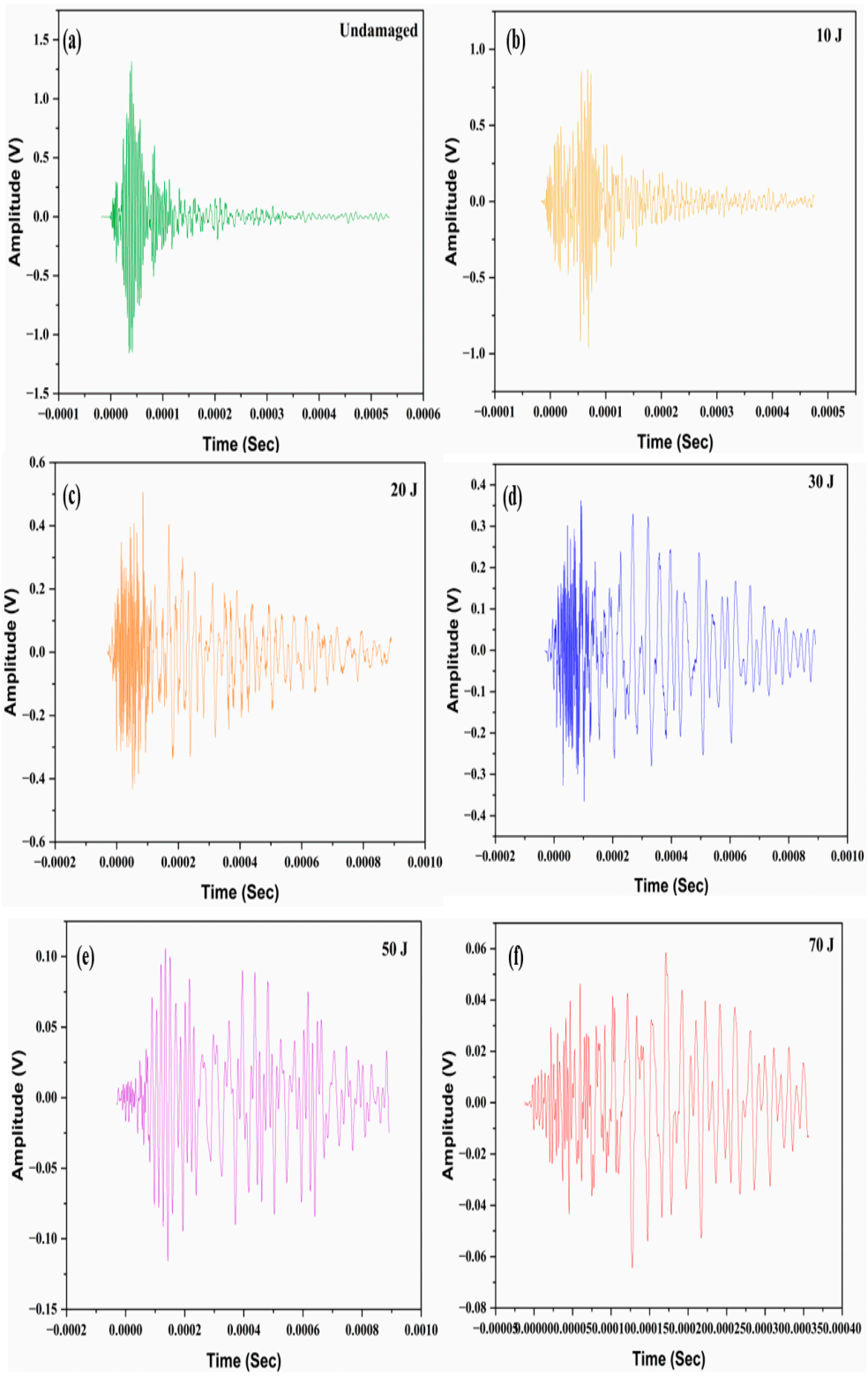

Figure 6. AU waveform for CFRP investigated at 30° for (**a**) Undamaged sample; (**b**) 10 J impacted sample; (**c**) 20 J impacted sample (**d**) 30 J impacted sample; (**e**) 50 J impacted sample; (**f**) 70 J impacted sample.

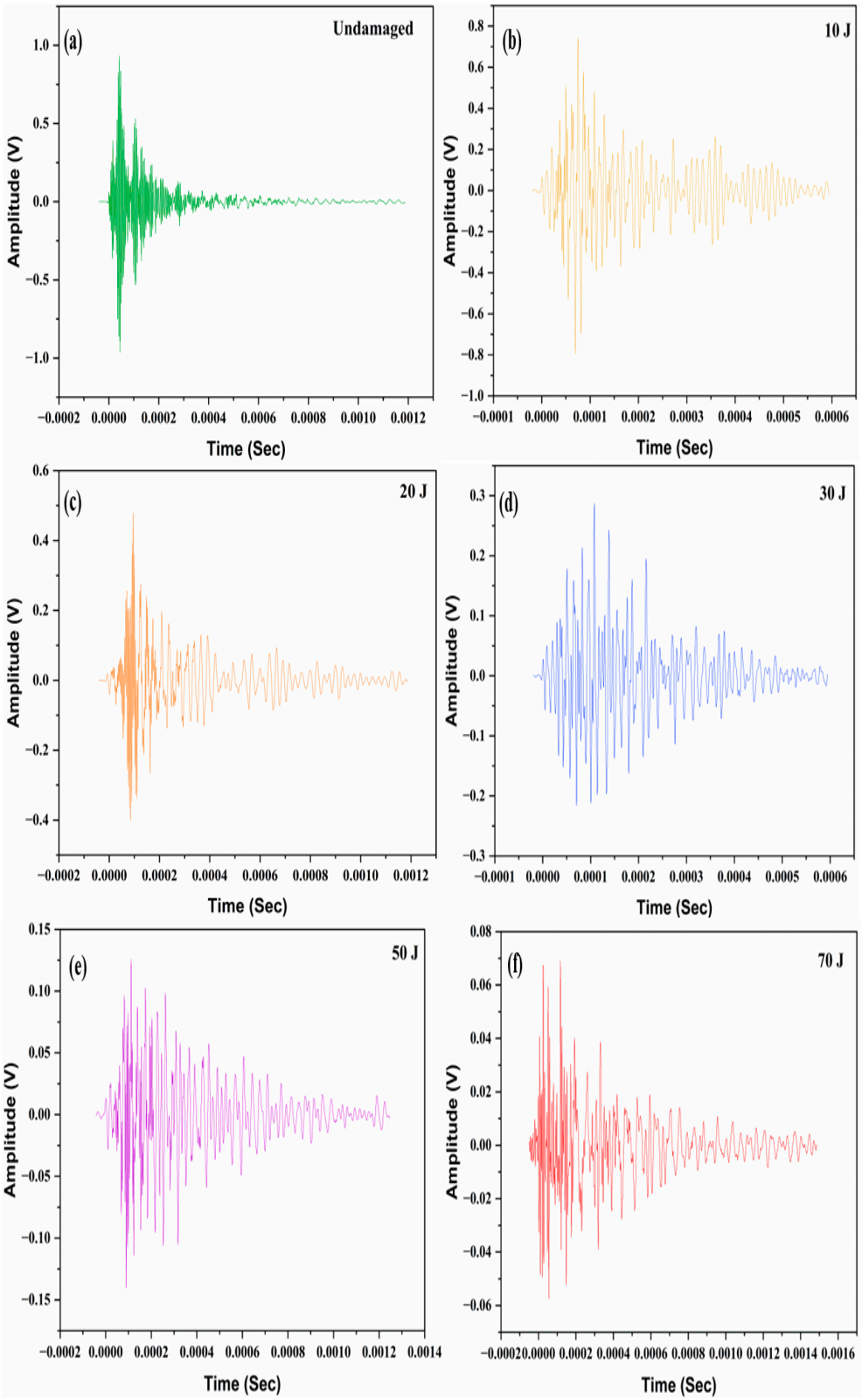

Figure 7. AU waveform for CFRP investigated at 45° for (**a**) Undamaged sample; (**b**) 10 J impacted sample; (**c**) 20 J impacted sample (**d**) 30 J impacted sample; (**e**) 50 J impacted sample; (**f**) 70 J impacted sample.

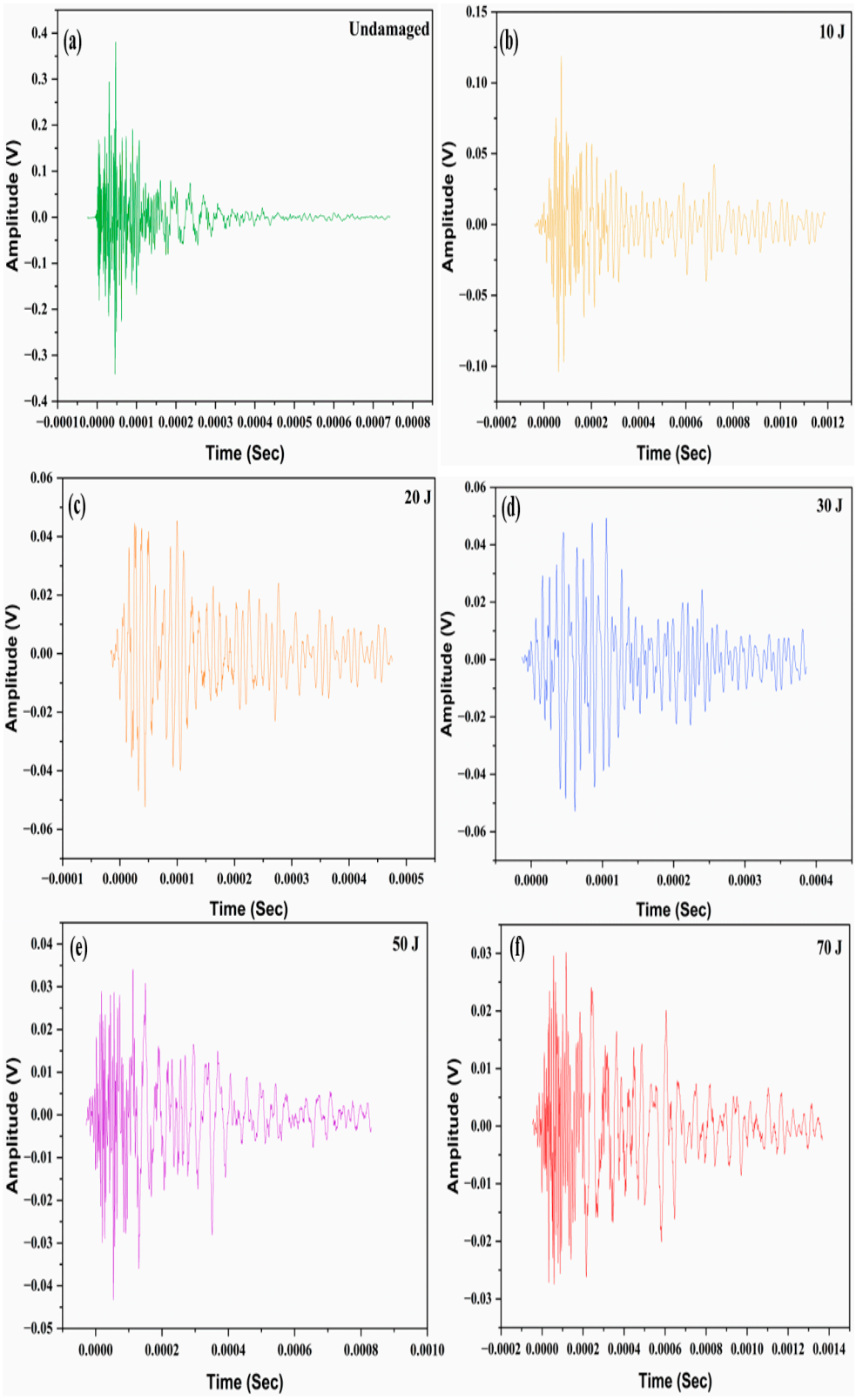

Figure 8. AU waveform for CFRP investigated at 60° for (**a**) Undamaged sample; (**b**) 10 J impacted sample; (**c**) 20 J impacted sample (**d**) 30 J impacted sample; (**e**) 50 J impacted sample; (**f**) 70 J impacted sample.

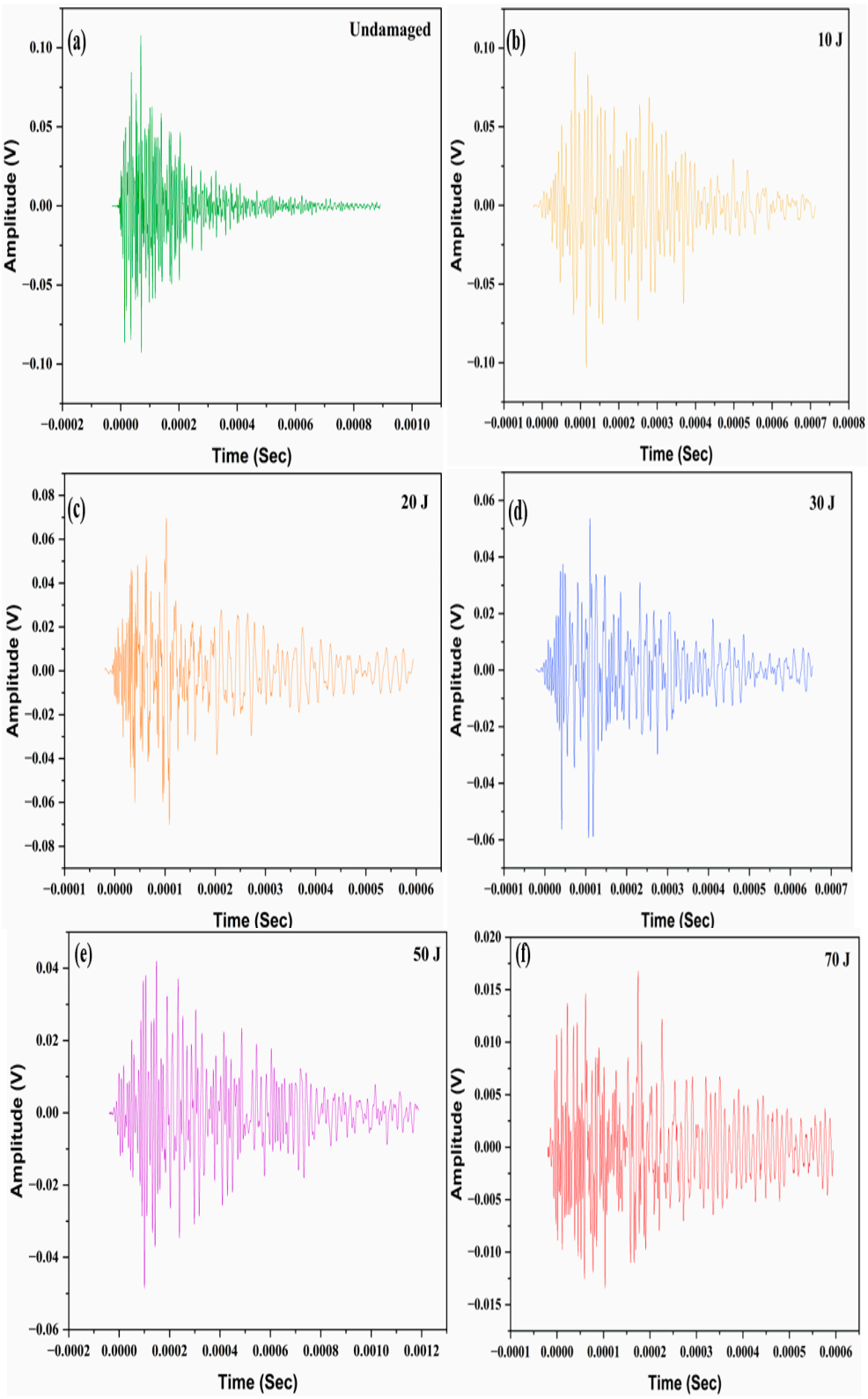

Figure 9. AU waveform for CFRP investigated at 90° for (**a**) Undamaged sample; (**b**) 10 J impacted sample; (**c**) 20 J impacted sample (**d**) 30 J impacted sample; (**e**) 50 J impacted sample; (**f**) 70 J impacted sample.

According to Lamb wave theory, it has been established that only the A0 and S0 wave modes propagate in thin plates at frequencies below 1 MHz [10,34]. The A0 wave mode

exhibits significant dispersion, making it unsuitable for the present investigation. Conversely, the S0 wave mode has less dispersion and demonstrates a stronger correlation with the stiffness of the medium [34]. Due to the increased phase velocity of the S0 wave mode at the frequencies of interest, it is easy to identify the leading section of the received signal as this waveform mode. Therefore, the S0 mode has been utilised here for further study, as the S0 mode is frequently regarded as more appropriate for damage detection in composite structures due to its lower dispersion and heightened sensitivity to specific types of damage, such as those induced by impact [12]. This characteristic makes the S0 mode particularly effective in identifying and characterising damage within composite materials. By monitoring the S0 mode, it was observed that the peaks for the undamaged CFRP were highest, with an amplitude of 2.91 V at an azimuthal angle of 0° (Figure 5a). This can be attributed to the fact that at an angle of 0°, the AU waves possess higher energy. As the measurement shifts towards higher azimuthal angles, the wave loses energy due to not propagating in the direction of the fibre orientation. The orientation of carbon fibres in CFRP significantly affects the propagation of AU waves, due to the anisotropic nature of the composite material. As the propagation direction deviates from the fibre orientation, the waves encounter more resistance, leading to energy dissipation. This misalignment reduces the amplitude of the AU waves. For example, at 90° (Figure 9a), where the wave propagation is perpendicular to the fibre direction, there is significant energy loss, evidenced by a 96.29% decrease in amplitude when compared with the angle at 0° (Figure 5a). Not only for the undamaged CFRP, but also for the AU waveforms following each impact energy level from 10 to 70 J, a gradual decrease in amplitude can be observed from azimuthal angle of 0° to 90°. This trend indicates that as the measurement angle increases, the AU wave loses energy, reflecting a consistent decline in amplitude across all impact energy levels.

Examining the impact-specific behaviour at a particular azimuthal angle reveals that both the peak amplitude and wave velocity of the AU signal decreased at 0°, as the impact energy and damage severity increased. Conversely, the time of arrival (TOA) of the AU signal increased. For example, the peak amplitude and TOA for undamaged CFRP were 2.91 V and 23.9 μsec, respectively (Figure 5a), which changed to 0.0567 V and 127.9 μsec for the 70 J impacted laminate (Figure 5f). Similar trends were observed at other azimuthal angles. At the 30°, 45°, 60° and 90° angles, the peak amplitude decreased by 95.64, 92.86, 92.12 and 85.14%, respectively at 70 J impact energy. Correspondingly, the TOA increased with impact energy by 284.53, 177.12, 149.36 and 152.75%, respectively, from the undamaged state to the 70 J impact condition. The increase in TOA with each increment in damage severity and higher impact loading indicates that the AU wave velocity is decreasing. This decrease in wave velocity is attributed to the wave traversing through the damaged zone.

When CFRP is subjected to an impact, it can suffer various forms of damage including matrix cracking, fibre breakage, delamination and debonding at the fibre–matrix interface. These damage mechanisms create discontinuities and inhomogeneities within the material. Damage within the composite introduces regions where the wave encounters interfaces between damaged and undamaged areas. These interfaces cause scattering and reflection of the wave energy, which disrupts the direct path of the wave, causing the AU waves to slow down as they propagate through the compromised areas and decrease the wave velocity.

Similarly, Figures 10–14 depict AU signals for FFRP composites, investigated at azimuthal angles ranging from 0° to 90°, respectively. Each Figure includes multiple plots: Figure 10a–14a show the signal for the undamaged sample, while Figures 10b–f–14b–f depict the signals corresponding to impact energies of 10, 20, 30, 50 and 70 J, respectively.

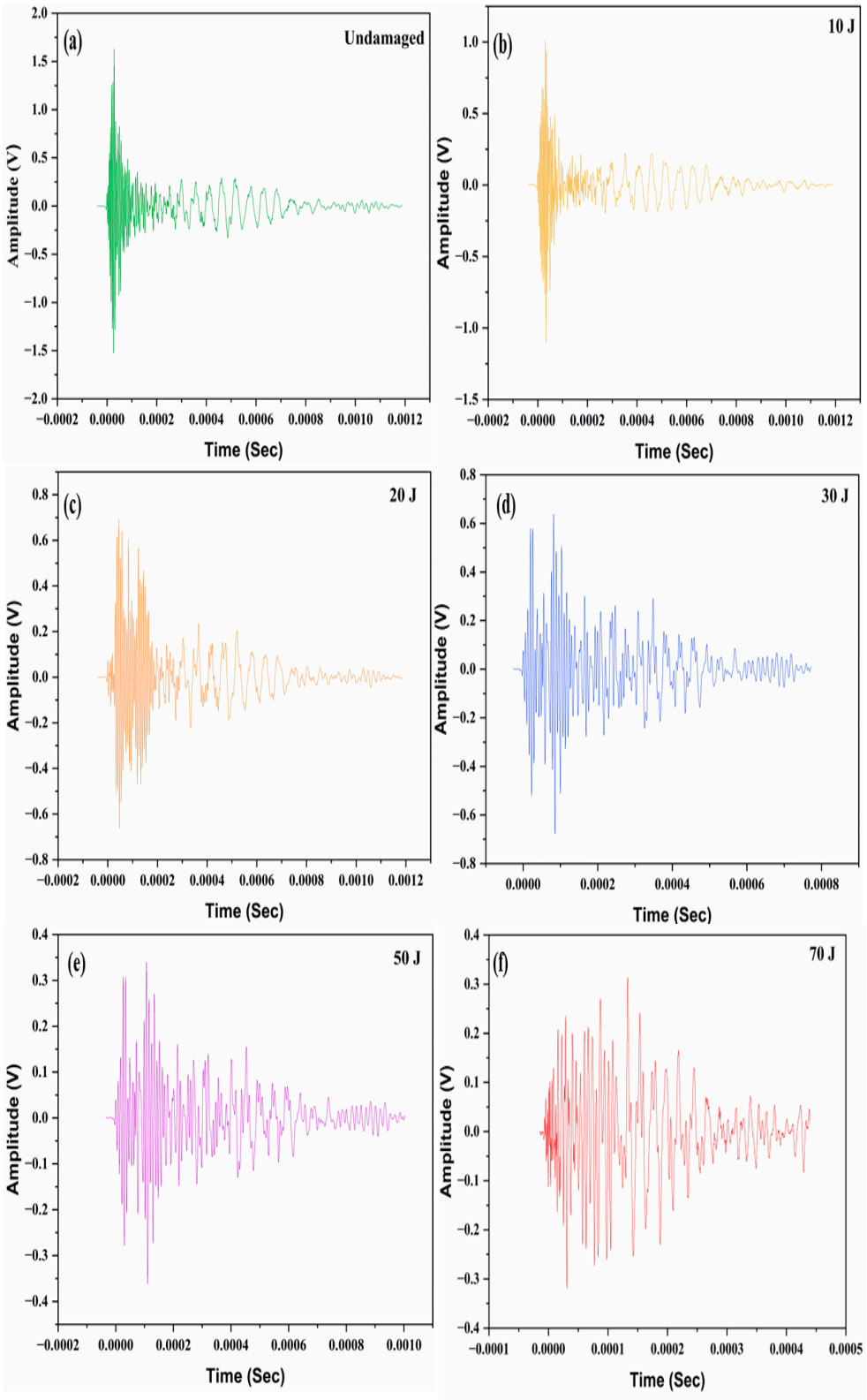

Figure 10. AU waveform for FFRP investigated at 0° for (**a**) Undamaged sample; (**b**) 10 J impacted sample; (**c**) 20 J impacted sample (**d**) 30 J impacted sample; (**e**) 50 J impacted sample; (**f**) 70 J impacted sample.

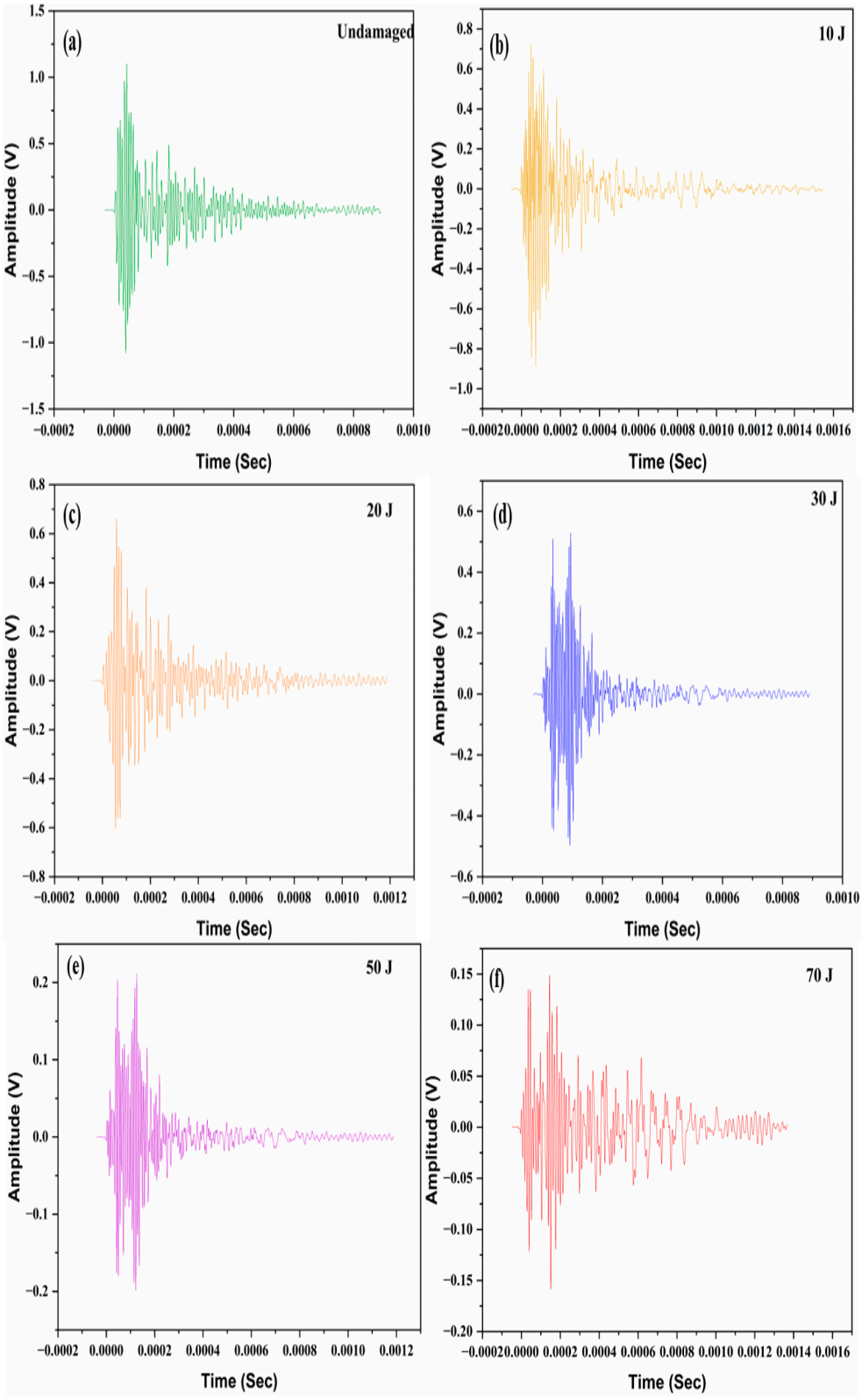

Figure 11. AU waveform for FFRP investigated at 30° for (**a**) Undamaged sample; (**b**) 10 J impacted sample; (**c**) 20 J impacted sample (**d**) 30 J impacted sample; (**e**) 50 J impacted sample; (**f**) 70 J impacted sample.

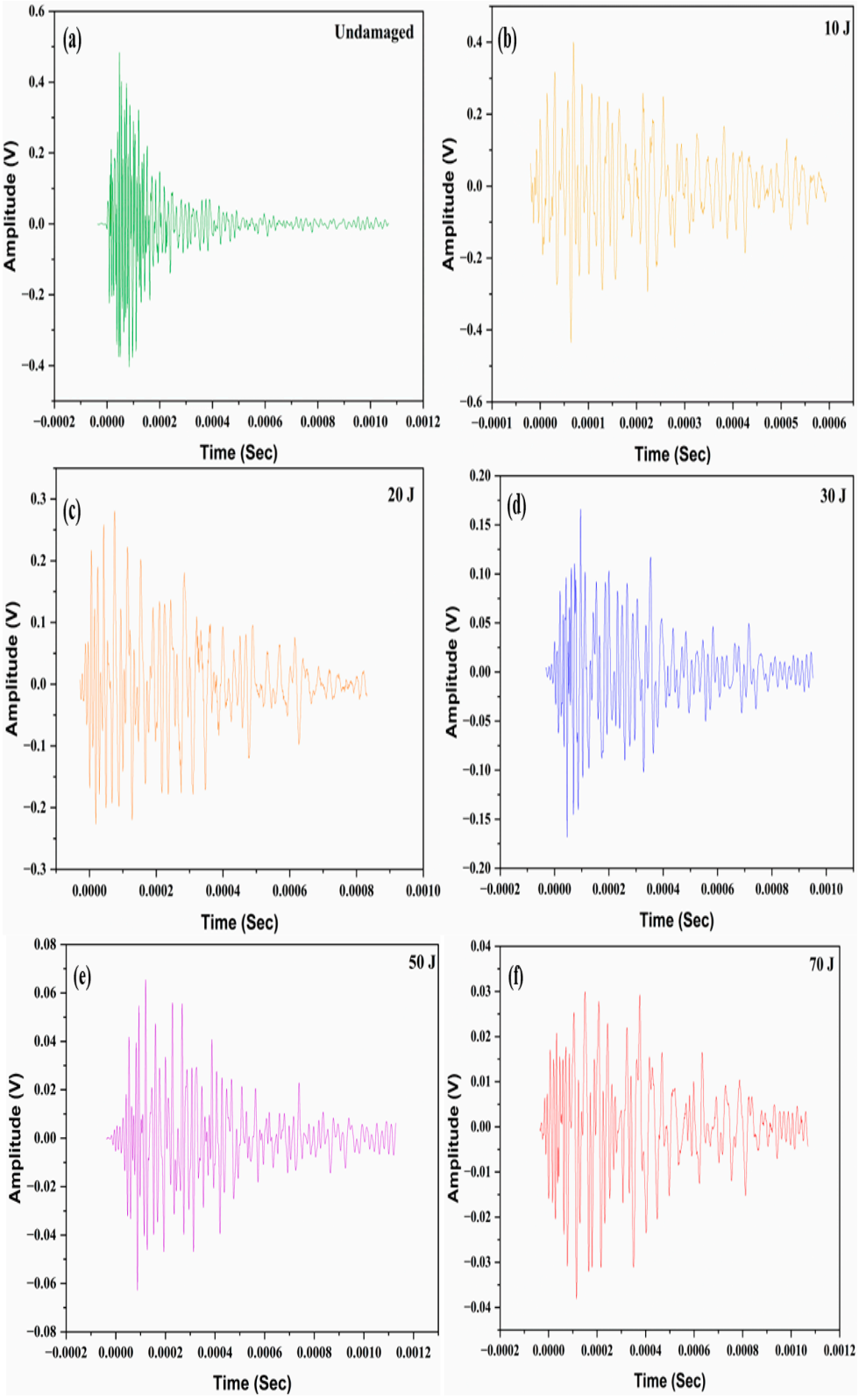

Figure 12. AU waveform for FFRP investigated at 45° for (**a**) Undamaged sample; (**b**) 10 J impacted sample; (**c**) 20 J impacted sample (**d**) 30 J impacted sample; (**e**) 50 J impacted sample; (**f**) 70 J impacted sample.

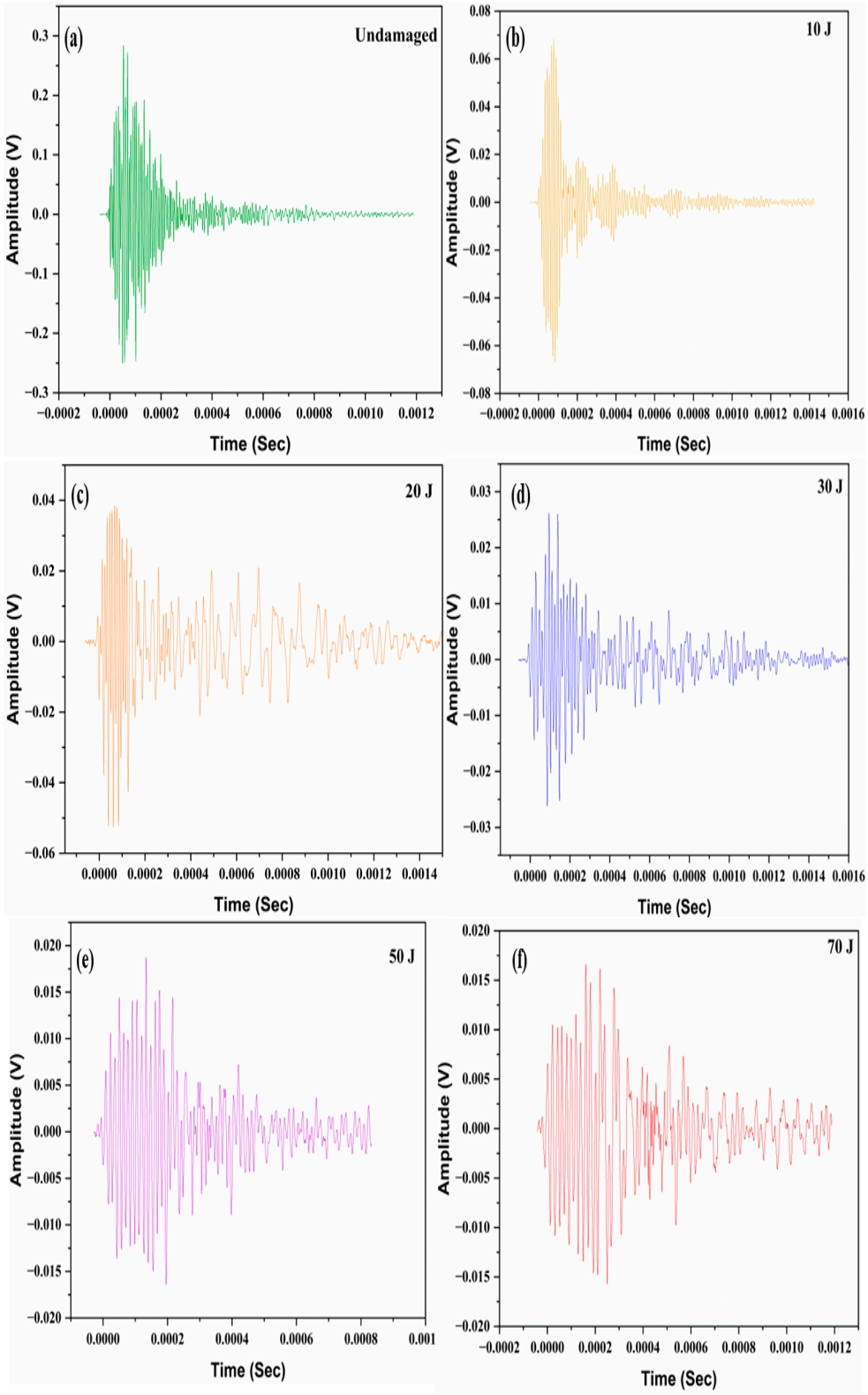

Figure 13. AU waveform for FFRP investigated at 60° for (**a**) Undamaged sample; (**b**) 10 J impacted sample; (**c**) 20 J impacted sample (**d**) 30 J impacted sample; (**e**) 50 J impacted sample; (**f**) 70 J impacted sample.

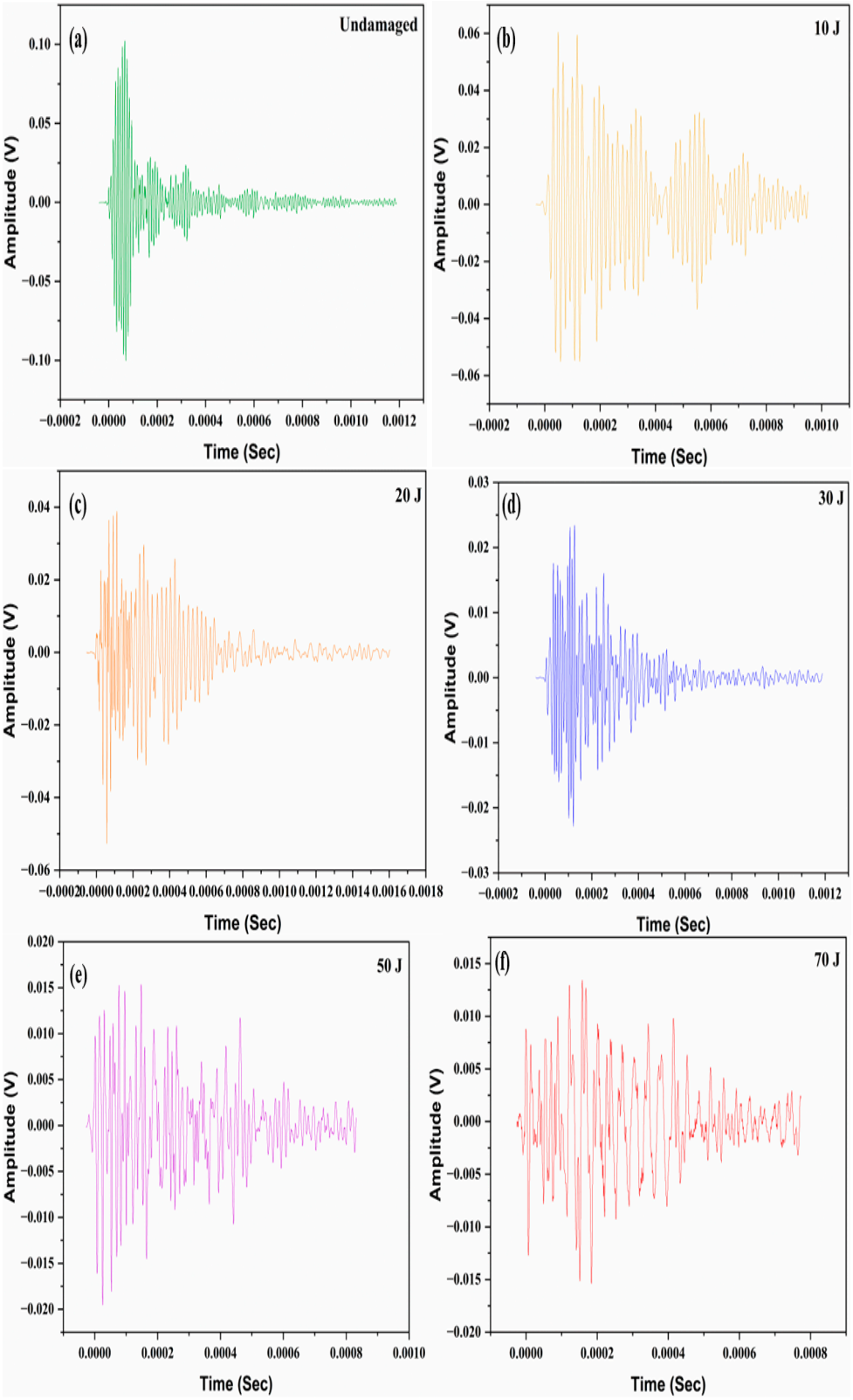

Figure 14. AU waveform for FFRP investigated at 90° for (**a**) Undamaged sample; (**b**) 10 J impacted sample; (**c**) 20 J impacted sample (**d**) 30 J impacted sample; (**e**) 50 J impacted sample; (**f**) 70 J impacted sample.

Unlike CFRP, the signals for FFRP exhibit more dispersion. This increased dispersion can be attributed to the material properties of the natural fibre, which result in higher attenuation. Although FFRP follows a trend that is similar to CFRP, the peak amplitude and wave velocity for FFRP are significantly lower. Conversely, the TOA is higher for FFRP, indicating a delay in the wave propagation, due to increased material damping and scattering effects.

For 0°, 30°, 45°, 60° and 90°, the peak amplitude decreases by 80.94, 87.15, 95.83, 94.28 and 87.12%, respectively, from the undamaged state to the 70 J impact energy. This decrease in amplitude is less pronounced when compared with CFRP. For instance, at 0°, CFRP shows a reduction of 96.29% (Figure 5), while FFRP shows a reduction of 80.94% (Figure 10). The natural fibre, such as flax, absorbs the signal more, resulting in a less significant change in signal amplitude. However, an 80% change is still quite significant for characterising damage modes in natural FRP, using AU testing.

The same trends are observed for wave velocity and TOA. The changes are quite significant, indicating that in natural fibre composites (NFCs), such as FFRP material properties cause higher attenuation and dispersion. These characteristics mean that TOA and wave velocity changes are more pronounced and variable, making them effective for detecting and characterising damage in natural fibres, using AUT [35]. The TOA increases from 288 μs (Figure 10a) to 1332 μs (Figure 10f) at 0°, establishing the impact of damage on signal propagation. This trend of increasing TOA with increasing impact energy is consistent across other azimuthal angles in this current study, further demonstrating the sensitivity of AU technique in assessing damage severity in natural FRP composites.

The higher TOA values and lower wave velocities in FFRP, when compared with CFRP, underscore the importance of considering material-specific properties when employing AU technique for SHM. These observations highlight the effective application of AU waveform indices in detecting and characterising damage within FFRP laminates, offering valuable insights for the design and maintenance of composite structures.

Finally, Figures 15–19 present the AU waveform analyses for the carbon/flax HFRP. Observing the peak amplitude of the signals, for instance, the HFRP composite at 0° shows a peak amplitude of 2.30 V (Figure 15a), which lies between the values observed for CFRP (2.91 V, Figure 5a) and FFRP (1.627 V, Figure 10a). This trend is consistent across all azimuthal angles and impact loadings.

One notable and interesting observation is that despite being a HFRP composite, as the azimuthal angle increases from 0° to 90°, the peak amplitude of the signal and the overall behaviour of the waveform shift from values characteristic of CFRP towards those of flax fibre. For example, at the 90°, the peak amplitude for the HFRP composite is 0.101 V, which is very close to the value observed from FFRP at the same angle. This indicates that the influence of the flax fibre becomes more pronounced at higher azimuthal angles, leading to similar attenuation and dispersion effects.

One possible explanation for this observed behaviour is the trade-off between elastic modulus and damping capacity in composite laminates, which is influenced by the fibre orientation [36,37]. Flax fibres, known for their superior damping properties, exhibit more pronounced damping effects as the orientation shifts from 0° to 90°. This shift alters the stiffness-damping relationship within the composite material. Consequently, as the damping properties become more dominant from 0° to 90°, the AU wave behaviour increasingly resembles that of the flax fibre. This trend indicates that the damping capacity of flax fibres significantly impacts the AU waveform, leading to increased attenuation and dispersion, particularly at higher azimuthal angles.

This shift in signal behaviour with increasing azimuthal angle highlights the complex interaction between the carbon and flax fibres within the hybrid composite. It suggests that the hybrid nature of the material introduces a blend of properties from both

constituent fibres, resulting in unique wave attenuation and dispersion characteristics. These findings underscore the importance of considering the hybrid composition in the SHM of composites, as the AU waveform indices provide critical insights into the damage detection and characterisation capabilities of AU testing.

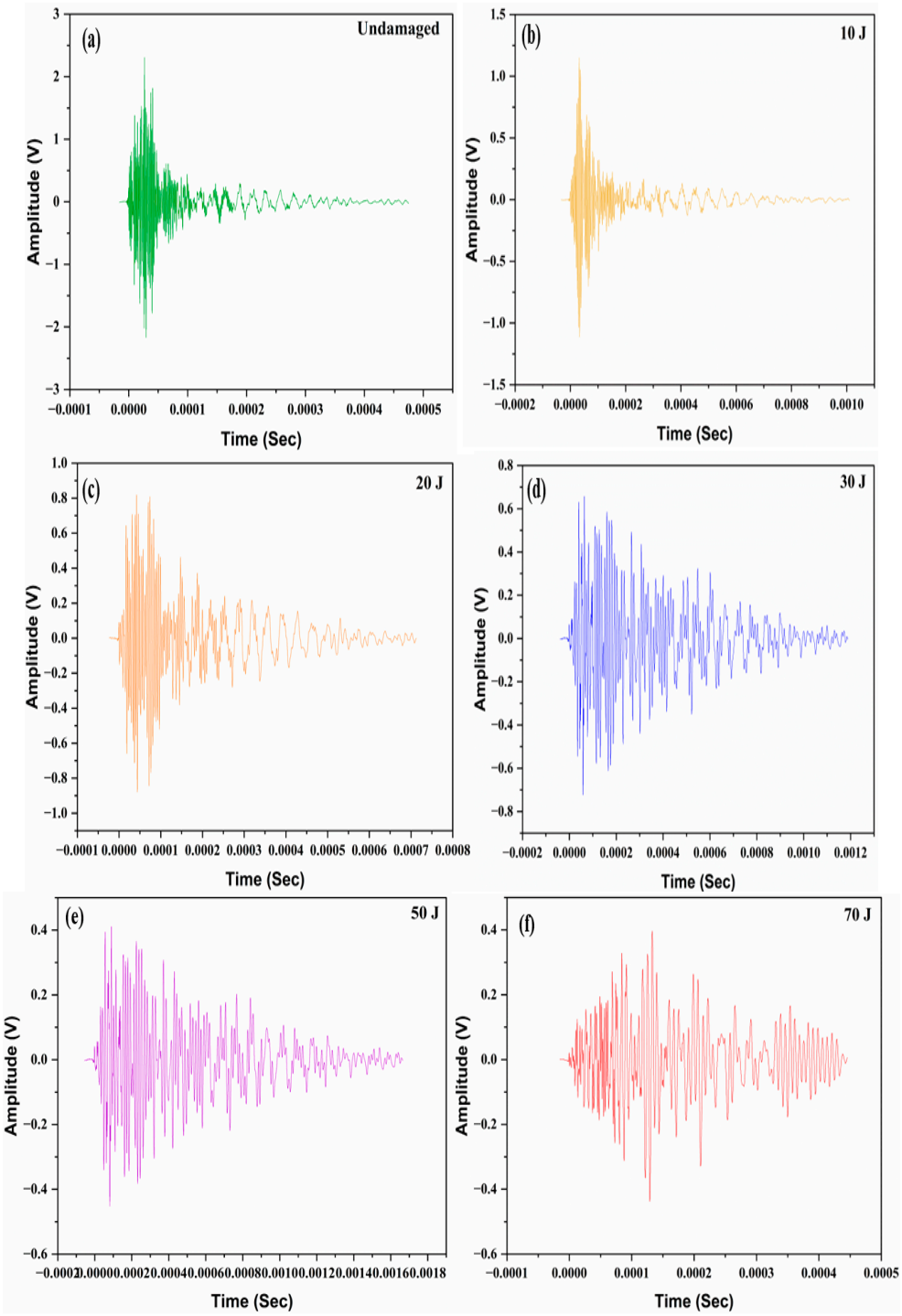

Figure 15. AU waveform for HFRP composite investigated at 0° for (**a**) Undamaged sample; (**b**) 10; (**c**) 20 J; (**d**) 30 J; (**e**) 50; (**f**) 70 J; impacted sample.

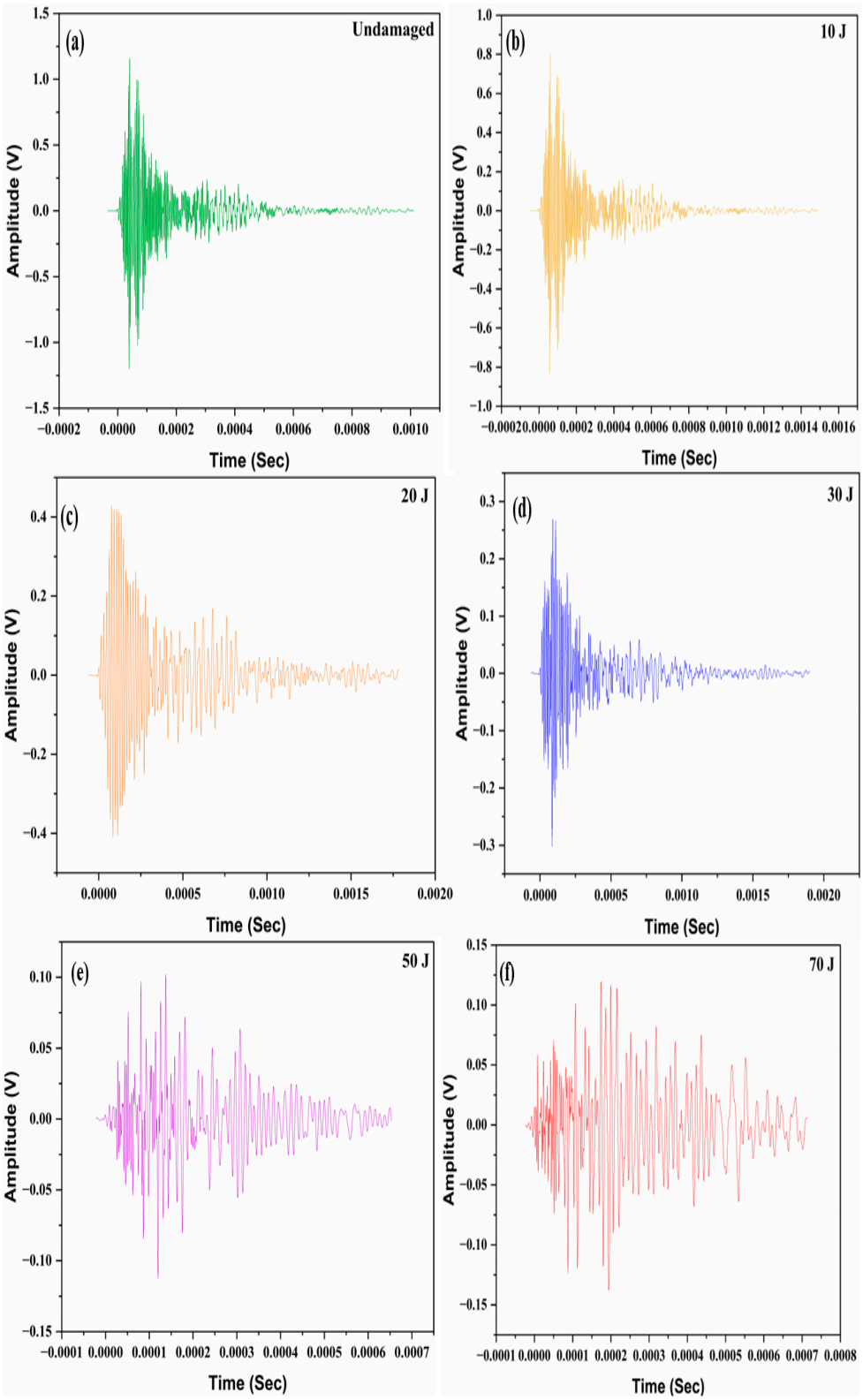

Figure 16. AU waveform for HFRP composite investigated at 30° for (**a**) Undamaged sample; (**b**) 10 J impacted sample; (**c**) 20 J impacted sample (**d**) 30 J impacted sample; (**e**) 50 J impacted sample; (**f**) 70 J impacted sample.

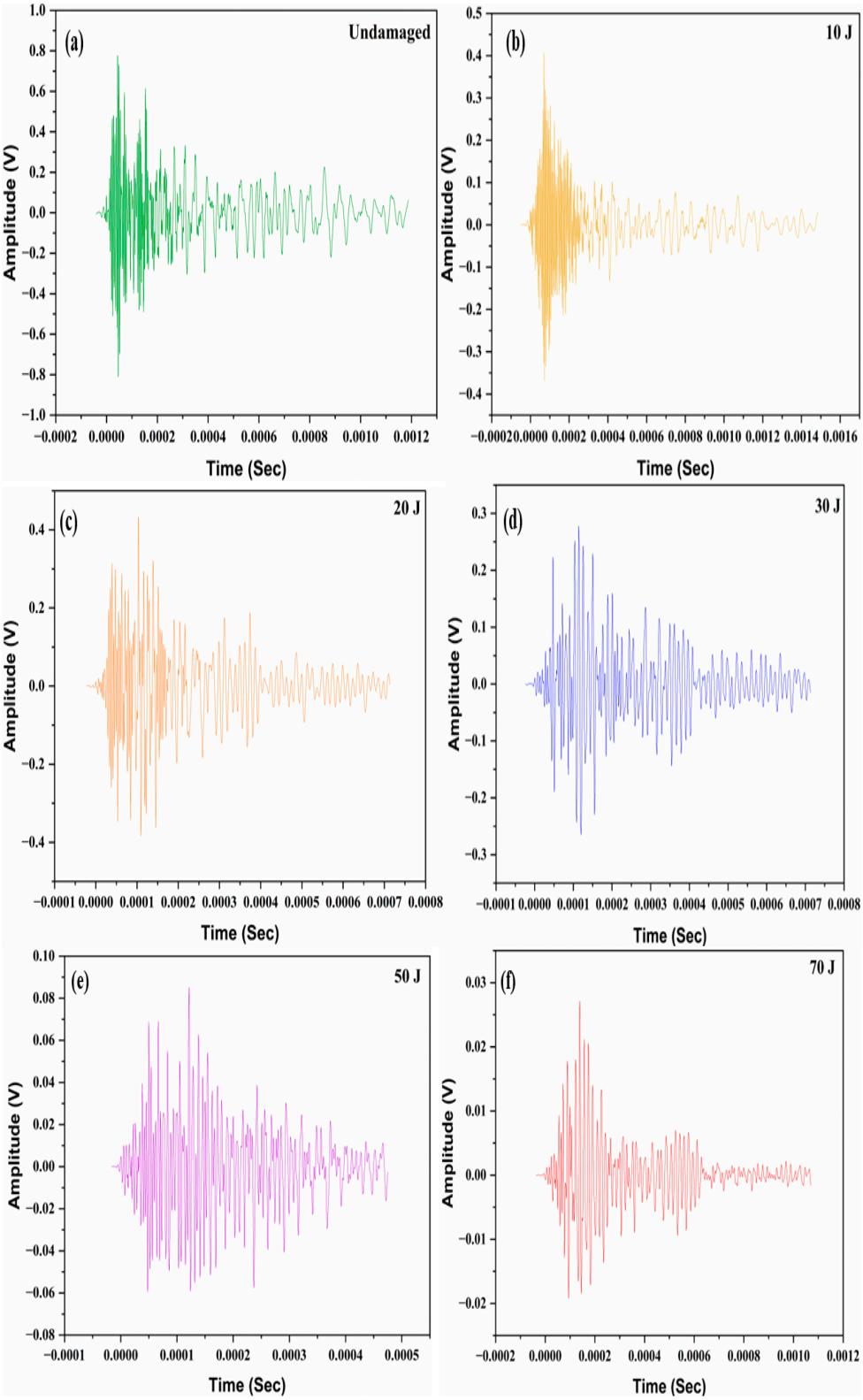

Figure 17. AU waveform for HFRP composite investigated at 45° for (**a**) Undamaged sample; (**b**) 10 J impacted sample; (**c**) 20 J impacted sample (**d**) 30 J impacted sample; (**e**) 50 J impacted sample; (**f**) 70 J impacted sample.

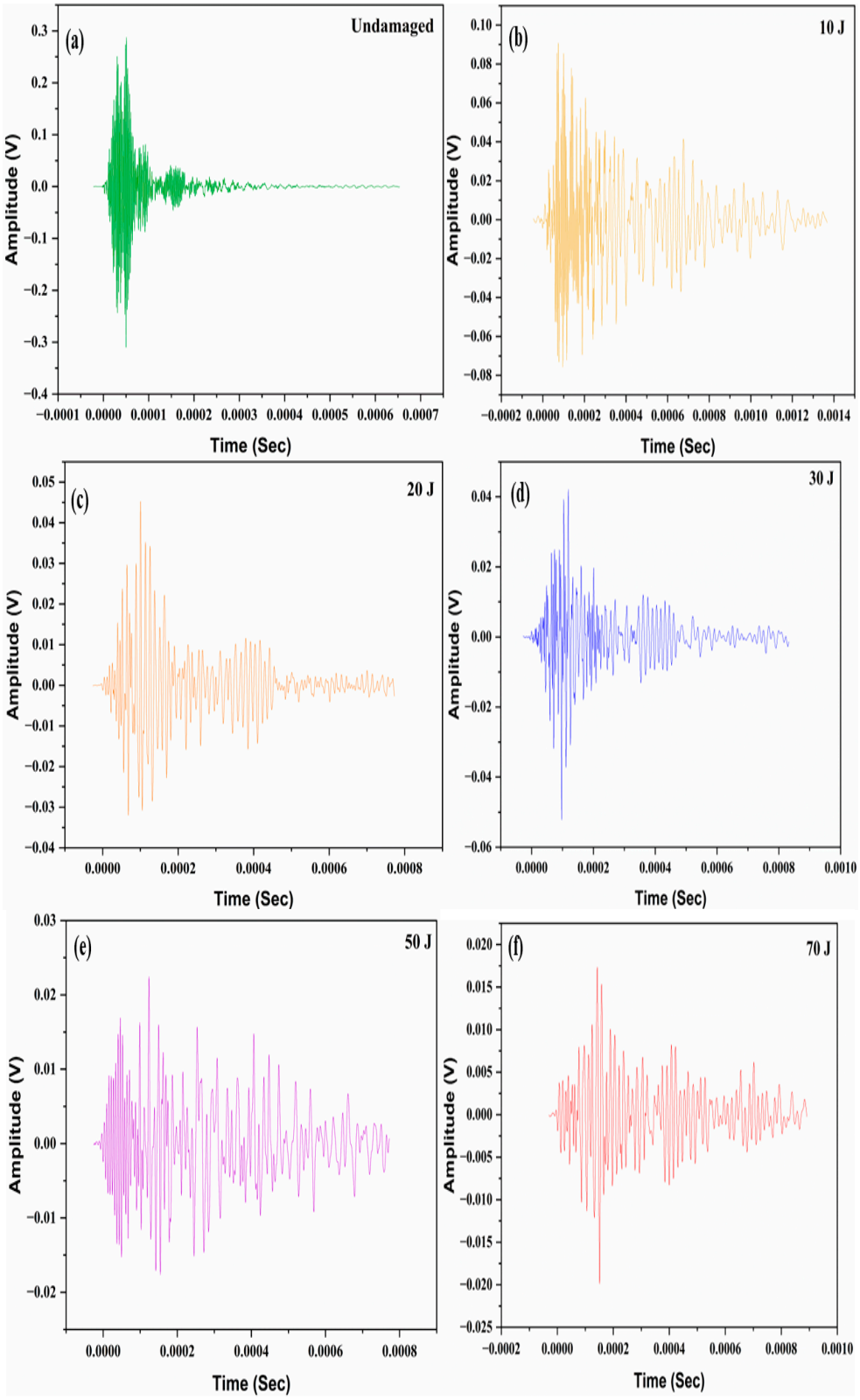

Figure 18. AU waveform for HFRP composite investigated at 60° for (**a**) Undamaged sample; (**b**) 10 J impacted sample; (**c**) 20 J impacted sample (**d**) 30 J impacted sample; (**e**) 50 J impacted sample; (**f**) 70 J impacted sample.

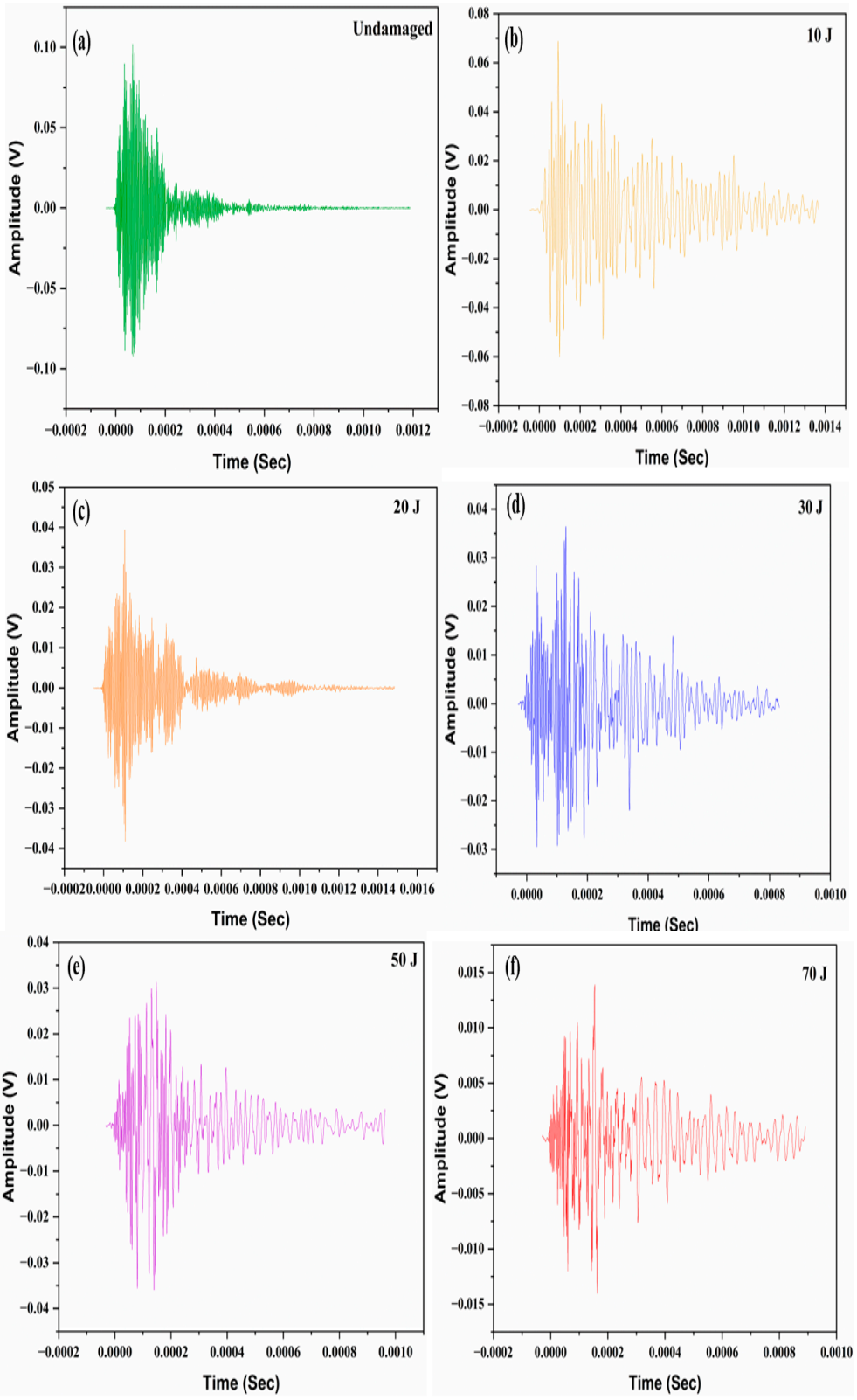

Figure 19. AU waveform for HFRP composite investigated at 90° for (**a**) Undamaged sample; (**b**) 10 J impacted sample; (**c**) 20 J impacted sample (**d**) 30 J impacted sample; (**e**) 50 J impacted sample; (**f**) 70 J impacted sample.

3.2. X-Ray Micro-CT and SEM Analyses

After the impact loading, fracture can occur due to the combination of various damage modes. Thus, to check the severity after each loading, an X-ray μCT scan, SEM and visual inspection were carried out after each impact level to check for the damage types, including matrix cracking, fibre breakage, fibre pull-out, delamination and fibre–matrix debonding caused by each loading, and to determine the dominant damage modes after impact loadings at different levels. Some of the scanned images are shown later with a summary of their analyses.

To start with, Figures 20–22 show the results of the visual inspection conducted on the impacted composite samples. The visual analysis indicates that the CFRP samples exhibit substantial resistance to impact damage, as no visible damage is observed. There is mainly barely visible damage, maintaining structural integrity up to an impact energy of 70 J. The hybrid carbon/flax/epoxy composites record similar resilience, although some signs of visible damage became evident at higher energy levels. In contrast, the flax/epoxy (FFRP) samples demonstrate progressive and significant visible damage as the impact energy increased, indicating lower resistance to mechanical stress when compared with the other two composites.

Furthermore, X-ray μCT scans and SEM were used to examine internal damage mechanisms. CFRP composites show matrix cracking and delamination at lower impact energies, progressing to fibre pull-out and breaking at higher impact energies. FFRP composites display matrix cracking, debonding and delamination, with significant damage at higher impact energies. Hybrid composites demonstrate a combination of damage mechanisms, including matrix cracking, delamination, fibre breaking and pull-out, indicating the complexity of damage modes in the materials.

At higher impact energies of 50 (Figure 23) and 70 J, a more complex combination of damage modes is observed in the CFRP laminate. These include both matrix and fibre damage responses, with fibre pull-out and fibre breaking becoming predominant. Fibre pull-out occurs when the fibres are partially displaced from the matrix, indicating a significant loss of load transfer capability between the fibres and the matrix.

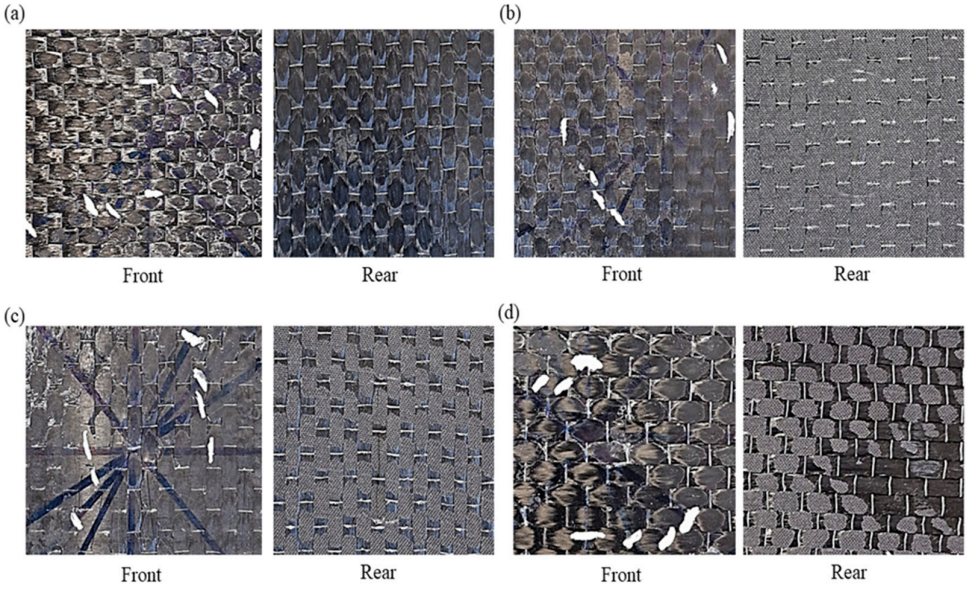

Figure 20. Visual inspection, showing front and rear views of CFRP at (**a**) 20, (**b**) 30, (**c**) 50 and (**d**) 70 J.

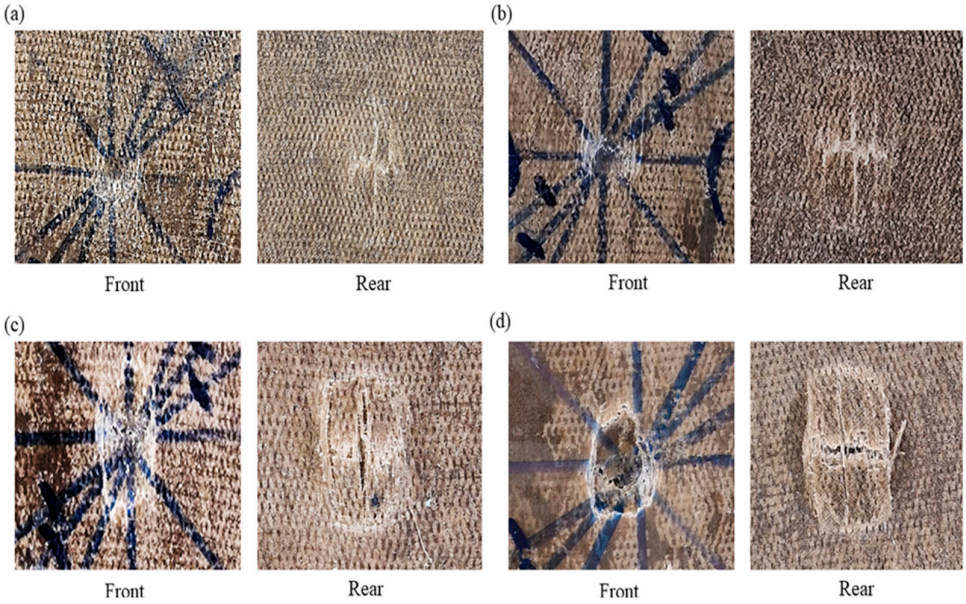

Figure 21. Visual inspection, depicting front and rear views of FFRP at (**a**) 20, (**b**) 30, (**c**) 50 and (**d**) 70 J.

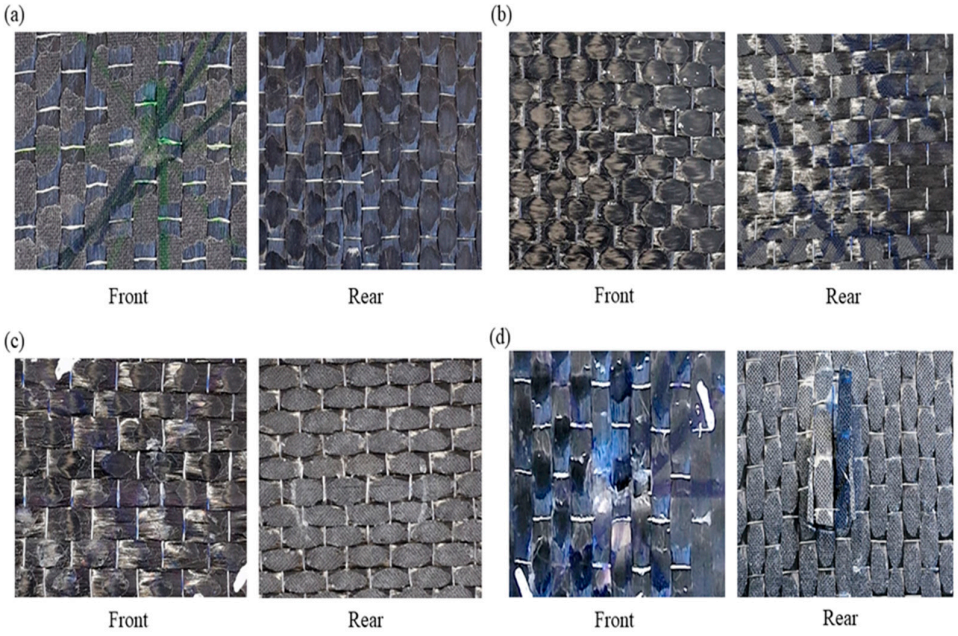

Figure 22. Visual inspection, showing front and rear views of HFRP composite at (**a**) 20, (**b**) 30, (**c**) 50 and (**d**) 70 J.

At an impact energy of 70 J, the damage mechanisms on FFRP composites are more complex, with fibre pull-out and delamination being the most prominent, as shown in the X-ray μCT micrograph in Figure 24. The SEM image after a 30 J impact (Figure 25a) on the HFRP composite shows the clusters of resin-rich zones and a good amount of delamination with some fibre pull-outs as well. The SEM image (Figure 25b) of the FFRP after a 30 J impact shows severe debonding and delamination. The magnification at 26×, with a scale bar of 1 mm, highlights the extensive separation between fibres and matrix, indicating significant structural compromise due to the impact.

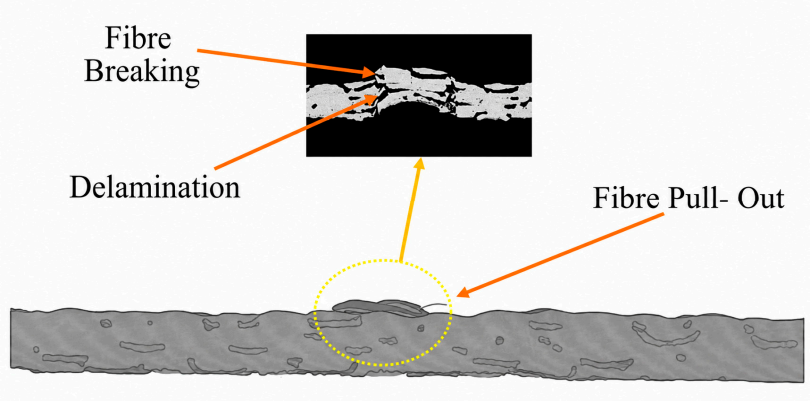

Figure 23. X-ray μCT scan after impact energy of 50 J on CFRP composite sample.

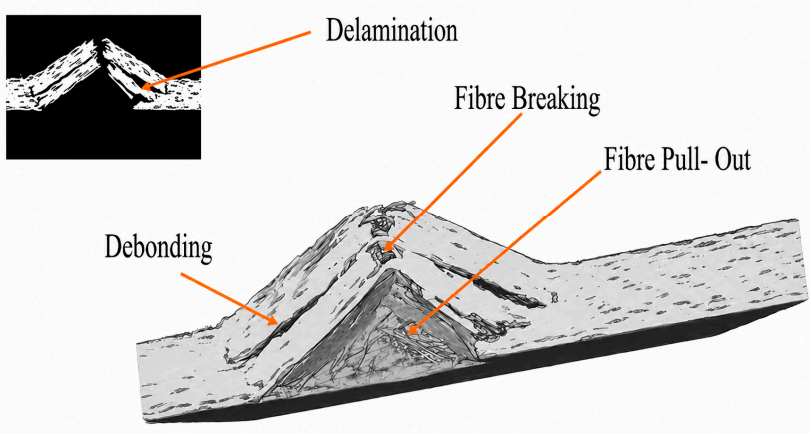

Figure 24. X-ray μCT image after impact energy of 70 J on FFRP composite sample.

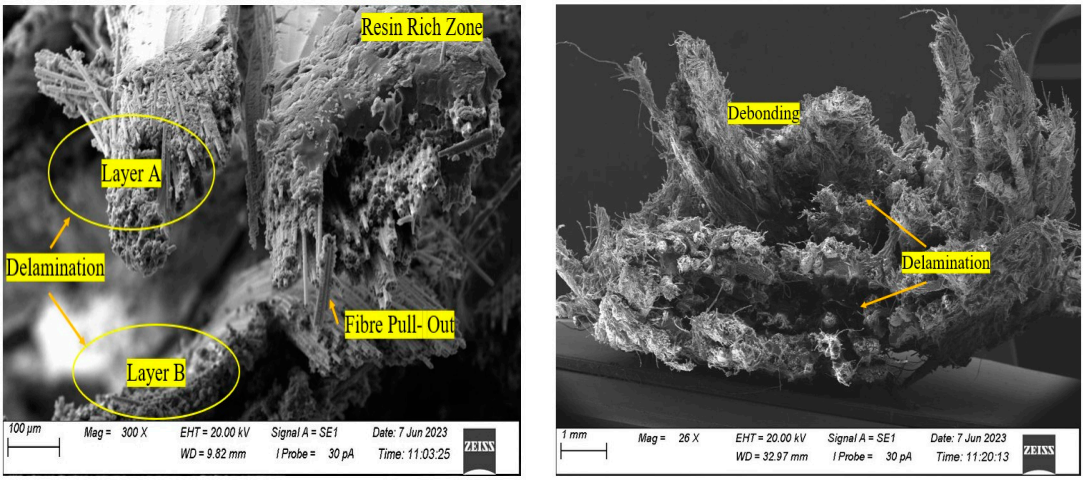

(**a**) (**b**)

Figure 25. SEM images of (**a**) carbon/ flax HFRP and (**b**) FFRP composites after impact energy of 30 J.

Table 2 presents a concise overview of the damage progression for each composite sample at different impact energy levels, summarising how each material responds to increasing impact energies.

Table 2. Summary of impact energy and corresponding damage modes for carbon, flax, and hybrid composite material.

Impact Energy (J)	CFRP)	FFRP	HFRP
10	Minor matrix cracking	Matrix cracking	Matrix cracking
20	Matrix debonding	Matrix cracking	Initial delamination
		Delamination	
30	Delamination	Dominant Delamination	Dominant Delamination
		Initial Fibre Breaking	
50	Fibre pull-out	Fibre breaking	Fibre breaking
	Fibre breaking	Perforation	Continued delamination
70	Severe fibre breaking	Fibre pull-out	Severe fibre pull-out
		Severe Delamination	Fibre Breaking

The damage progression summarised in Table 2 provides a physical basis for interpreting the AUWI trends. At lower impact energies, the dominant damage modes were matrix cracking, matrix debonding and initial delamination. These defects interrupt the continuity of the polymer–matrix and fibre–matrix interface, producing measurable reductions in peak amplitude and wave velocity. At higher impact energies, the damage state became multi-mechanistic, with fibre pull-out, fibre breakage, perforation and severe delamination introducing stronger scattering, reflection, attenuation and local stiffness degradation along the propagation path. The progressive reduction in AUWI1 and AUWI2 is therefore consistent with the transition from matrix-dominated damage to fibre- and delamination-dominated damage observed through visual inspection, X-ray micro-CT and SEM analyses.

The classifications of "initial" and "dominant" damage modes in Table 2 are based on qualitative interpretation of visual inspection, X-ray μCT and SEM observations, where "initial" refers to the first observable occurrence of a damage mode and "dominant" refers to the most visually and microscopically evident damage mechanism within the inspected region.

3.3. Extended Quantitative Analysis (AUWIs Correlated with Damage Severity)

In this study, both time-domain and frequency-domain parameters are utilised to comprehensively characterise damage, using AU testing. By examining a wide range of parameters, the study aimed to establish correlations with damage severity under controlled experimental conditions effectively. A clear trend is observed in the peak amplitude of the AU waveform and wave velocity within the studied frequency range, with changes in AUWI1 (peak amplitude) and AUWI2 (wave velocity), serving as indicators of damage severity. These indices are normalised by their undamaged state values and plotted against different impact energies to represent various damage levels.

AUWI3 measures the energy content, represented by the area under the power spectral density (PSD) distribution function. AUWI4 assesses the central frequency, or the energy-weighted average frequency, of the AU wave, using the entire PSD of the received wave for calculation. AUWI5 evaluates the skewness of the PSD distribution, indicating the anisotropy of the medium. A single peak in the power spectrum suggests resonance, whereas a flat spectrum indicates white noise. For Lamb waves propagating in an anisotropic and heterogeneous medium, the power spectrum lies between resonance and white noise. A skewness value (AUWI5) greater than 1.0 signifies significant skewness in the frequency content distribution, reflecting the anisotropic nature of the medium.

To avoid repetition in the material-specific AUWI discussion, the main percentage variations and adjusted R^2 trends are consolidated in Table 3. The subsequent discussion

focuses on the most relevant material-specific observations, while the comparative interpretation is developed in Section 3.4.

Table 3. Consolidated percentage variation and adjusted R^2 summary for AUWIs across CFRP, FFRP and HFRP composites.

Material	AUWI	Most Sensitive Azimuthal Angle	Maximum Percentage Change	Adjusted R^2 Trend	Interpretation
CFRP	AUWI1 Peak amplitude	0°	95.53% decrease	High	Strong attenuation response
	AUWI2 Wave velocity	0° and 45°	74.68% decrease	Highest overall	Strong stiffness-sensitive response
	AUWI3 Energy content	60° and 90°	93.75% decrease	Moderate to variable	Direction-dependent energy loss
	AUWI4 Centroid frequency	90°	22.22% decrease	Lower	Limited standalone sensitivity
	AUWI5 Skewness factor	90°	23.81% increase	Variable	Frequency asymmetry descriptor
FFRP	AUWI1 Peak amplitude	45°	94.94% decrease	High but variable	Strong attenuation response
	AUWI2 Wave velocity	0°	73.72% decrease	High	Strong damage-sensitive response
	AUWI3 Energy content	45°	88.00% decrease	Moderate	Energy loss affected by damping
	AUWI4 Centroid frequency	90°	14.28% decrease	Lower	Limited standalone sensitivity
	AUWI5 Skewness factor	45° and 60°	35.24% increase	Variable	Heterogeneity-sensitive descriptor
HFRP	AUWI1 Peak amplitude	30°	98.69% decrease	High	Strong hybrid attenuation response
	AUWI2 Wave velocity	45°	81.56% decrease	High	Strongest velocity response
	AUWI3 Energy content	90°	84.00% decrease	Moderate to low	Direction-dependent energy loss
	AUWI4 Centroid frequency	30°	31.63% decrease	Variable	Spectral redistribution descriptor
	AUWI5 Skewness factor	45°	44.23% increase	Variable	Strong frequency asymmetry response

The AUWIs for CFRP were evaluated (Figure 26) at azimuthal angles of 0°, 30°, 45°, 60° and 90° across various impact energies of 10 to 70 J and regression analysis was performed to check for their linearity. For CFRP composites, AUWI1 and AUWI2 exhibited the clearest damage-sensitive trends with increasing impact energy. Peak amplitude showed the strongest reduction at 0° and 30°, indicating that attenuation was most pronounced when the wave propagated along or close to the principal fibre direction. Wave velocity also decreased substantially, particularly at 0° and 45°, supporting its sensitivity to stiffness degradation and damage-induced discontinuities in the propagation path. AUWI3 showed substantial energy loss at higher azimuthal angles, while AUWI4 and AUWI5 exhibited smaller or more variable changes.

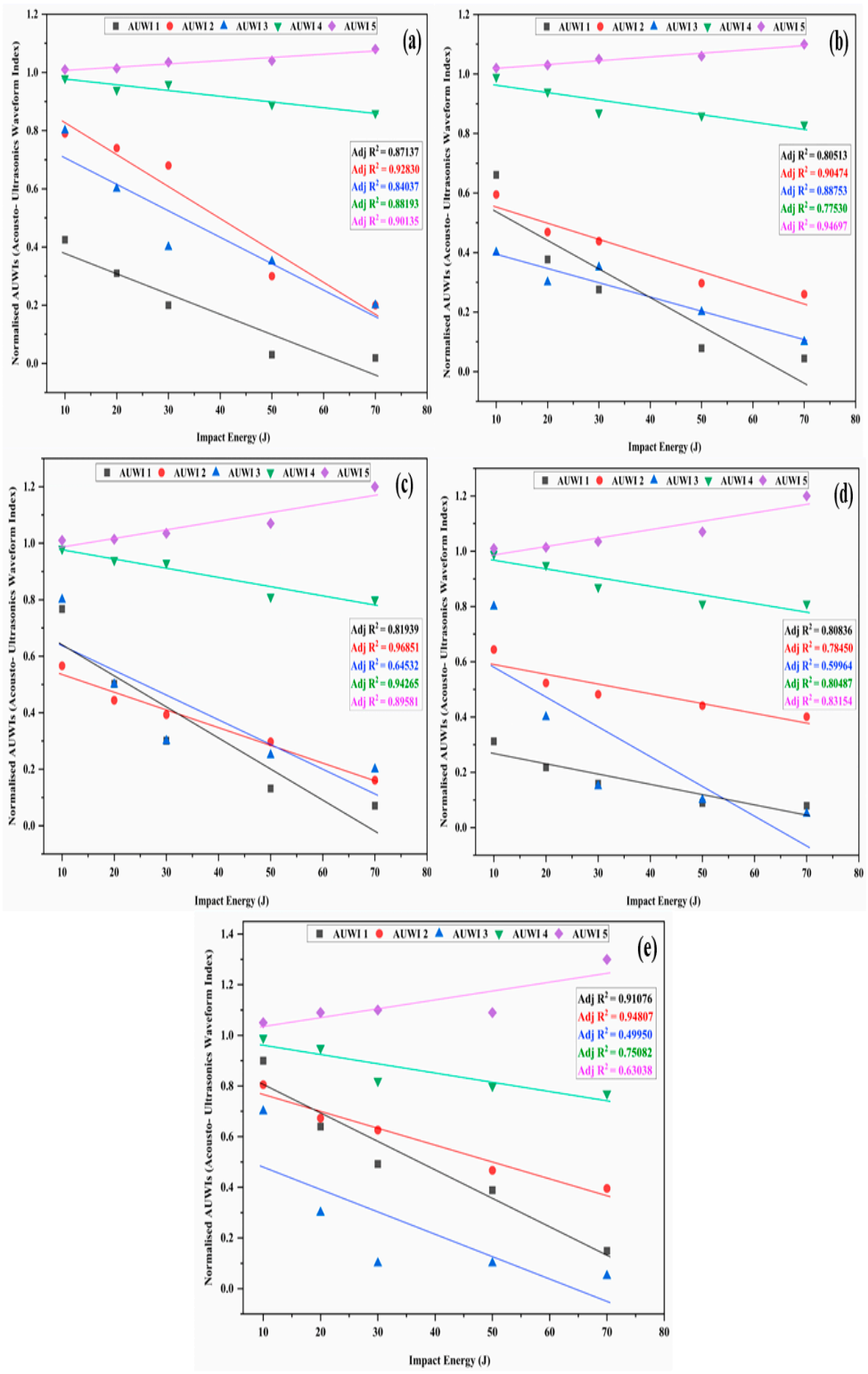

Figure 26. AUWIs for CFRP composites at (**a**) 0°, (**b**) 30°, (**c**) 45°, (**d**) 60° and (**e**) 90° azimuthal angles.

Figure 27 depicts the AUWIs for FFRP composite at various azimuthal angles of (a) 0°, (b) 30°, (c) 45°, (d) 60° and (e) 90°. For FFRP composites, the AUWI trends reflected the higher damping and attenuation characteristics of the natural fibre laminate. AUWI1 showed a strong reduction, particularly at 45°, while AUWI2 decreased most strongly at 0° and 30°. These results indicate that both amplitude loss and velocity reduction are

sensitive to impact-induced degradation in FFRP. AUWI3 also showed notable energy reduction, consistent with the higher wave absorption capacity of flax fibre composites. However, AUWI4 and AUWI5 showed more variable responses with azimuthal angle, indicating that frequency-domain features are influenced by the heterogeneous and damping-dominated nature of the natural fibre architecture.

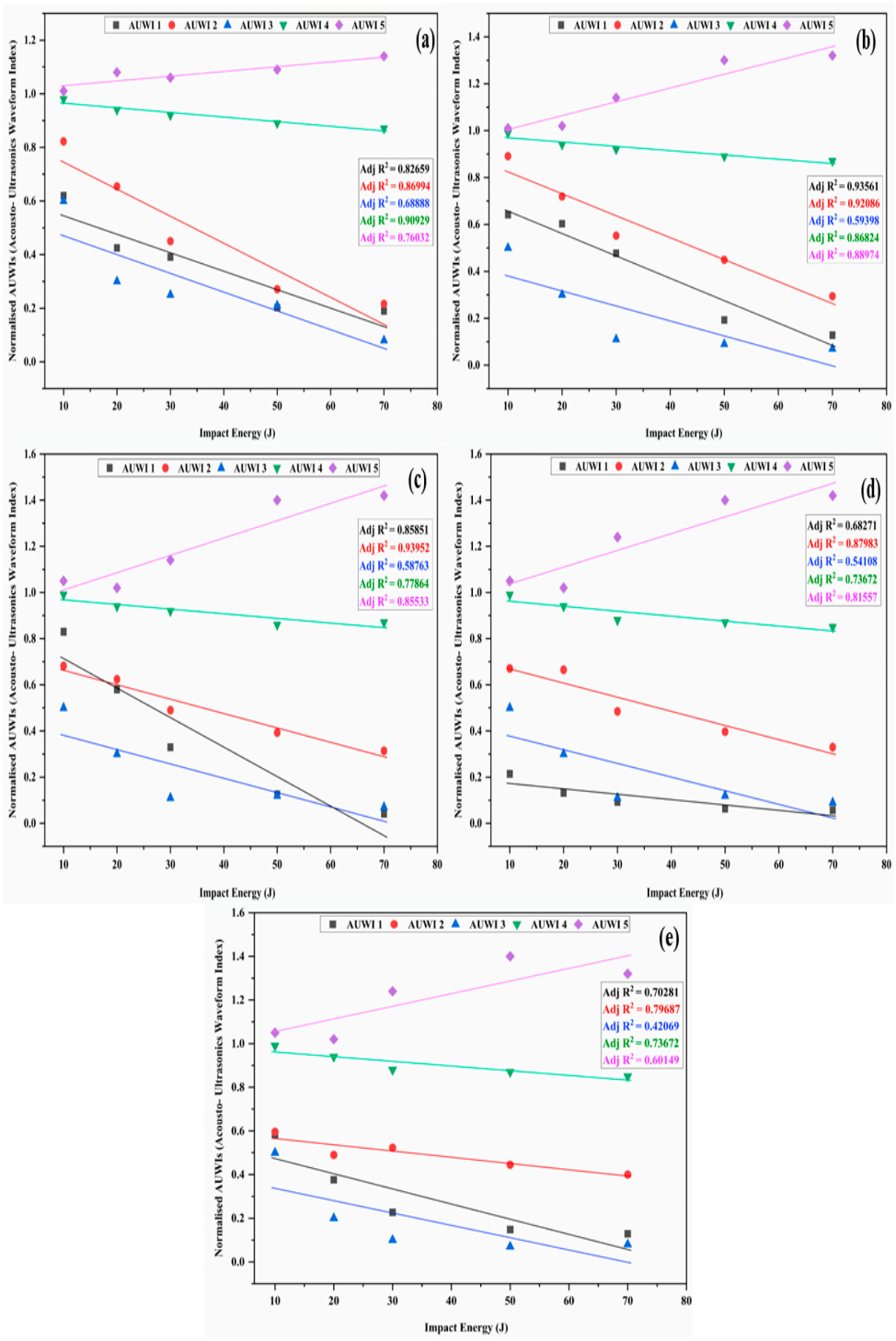

Figure 27. AUWIs for FFRP composites at (**a**) 0°, (**b**) 30°, (**c**) 45°, (**d**) 60°and (**e**) 90° azimuthal angles.

Figure 28 shows the AUWIs for the HFRP composite at different azimuthal angles of (a) 0°, (b) 30°, (c) 45°, (d) 60° and (e) 90°. For HFRP composites, AUWI1 and AUWI2 again provided the strongest indicators of increasing impact severity. Peak amplitude showed the highest reduction at 30°, while wave velocity showed the greatest reduction at 45°. This reflects the combined influence of carbon fibre stiffness and flax fibre damping within the hybrid laminate. AUWI3 showed direction-dependent energy loss, while AUWI4 and AUWI5 captured spectral redistribution and increased frequency-domain asymmetry, particularly at intermediate azimuthal angles. These results suggest that the hybrid architecture produces a more complex wave response than CFRP or FFRP alone, making complementary waveform descriptors useful for interpretation.

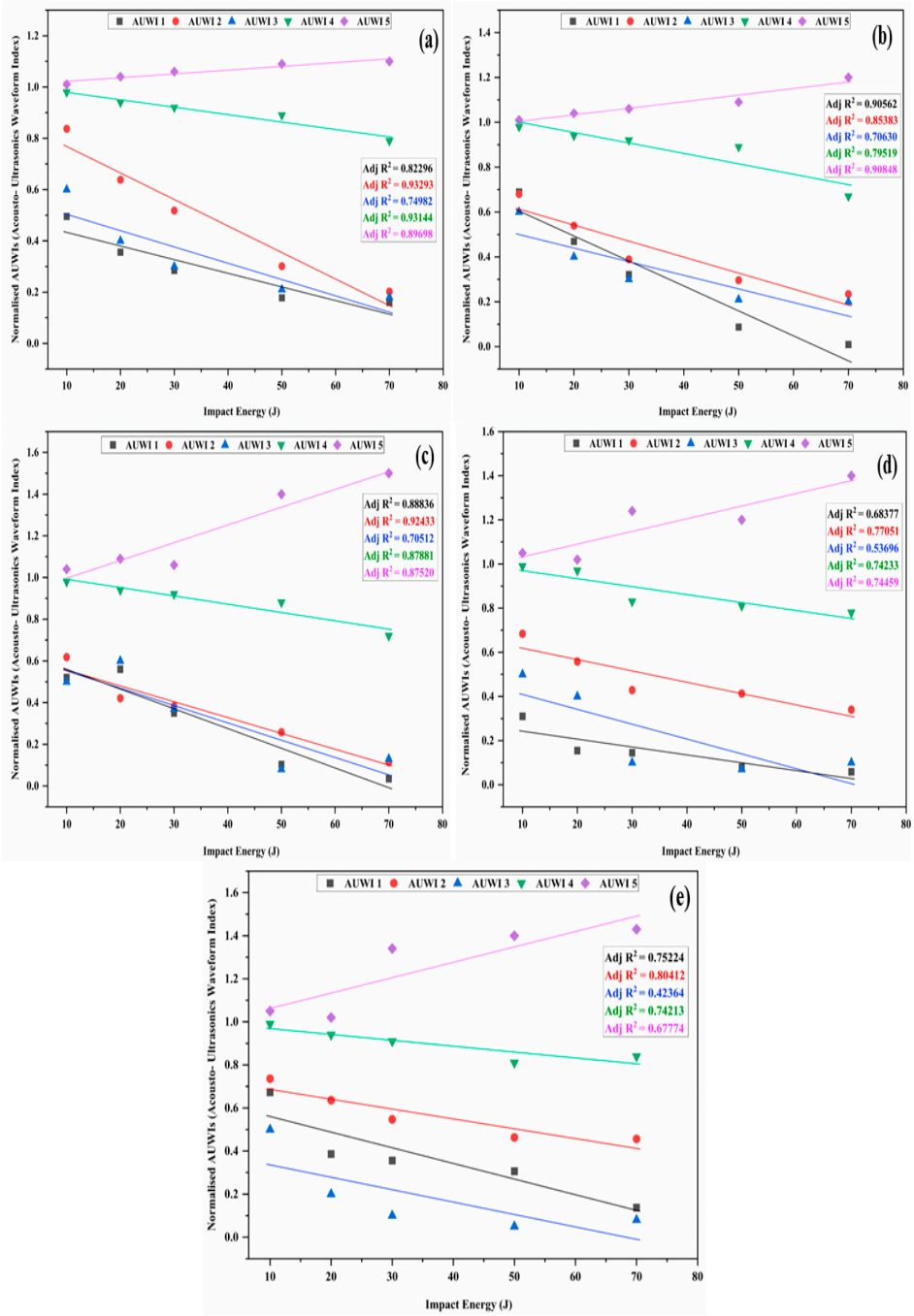

Figure 28. AUWIs for HFRP composite at (**a**) 0°, (**b**) 30°, (**c**) 45°, (**d**) 60° and (**e**) 90° azimuthal angles.

https://doi.org/10.3390/app16136313

3.4. Comparative Analysis of AUWIs for CFRP, FFRP and HFRP Composites

The AUWIs for CFRP, FFRP and HFRP composites were evaluated at azimuthal angles of 0°, 30°, 45°, 60° and 90° across various impact energies from 10 to 70 J.

For AUWI1 (Peak Amplitude), CFRP composite shows the most significant decrease at 0° (95.53%) and 30° (93.34%), indicating high sensitivity to impact damage near the fibre orientation. FFRP exhibits the greatest reduction at 45° (94.94%), suggesting higher sensitivity to damage when aligned with the fibre orientation. HFRP composite shows substantial decreases at 30° (98.69%) and 45° (93.27%), indicating high sensitivity to impact damage.

AUWI2 (Wave Velocity) reveals that CFRP composite had the largest reductions at 0° (74.68%) and 45° (71.55%), showing the orientations that are more susceptible to velocity changes. FFRP composite exhibits significant decreases at 0° (73.72%) and 30° (66.99%), highlighting sensitivity to damage. HFRP composite sample has the most considerable decrease at 45° (81.56%).

AUWI3 (Energy Content) demonstrates that CFRP has the highest reductions at 60° (93.75%) and 90° (92.86%), indicating substantial energy loss due to damage. FFRP records significant reductions at 30° and 45° (86% and 88%, respectively), while HFRP composite shows the most significant decreases at 45° (74%) and 60° (80%).

AUWI4 (Central Frequency) generally shows the smallest percentage of decrease, indicating less sensitivity to damage across all the composite samples. The highest reduction is observed in HFRP composite at 30° (31.63%).

AUWI5 (Skewness of PSD Distribution) increases with higher impact energies, with the most significant changes in HFRP composite at 45° (44.23%) and 60° (33.33%), reflecting its higher anisotropy and heterogeneity.

It should be noted that AUWI3, AUWI4 and AUWI5 did not show consistently high adjusted R^2 values across all material types and azimuthal angles. Therefore, these indices should not be interpreted as universally reliable standalone damage severity indicators. Their inclusion in the present study is justified because they provide complementary physical information about the received AU signal. AUWI3 represents the transmitted energy content and is related to attenuation and energy loss. AUWI4 describes redistribution of the spectral content, while AUWI5 reflects asymmetry of the frequency distribution associated with anisotropy and heterogeneous wave–damage interactions.

The lower adjusted R^2 values observed for some material–angle combinations indicate that these indices may have non-linear, direction-dependent or material-dependent responses to impact damage. This behaviour is particularly relevant in natural and hybrid FRP composites, where fibre–matrix heterogeneity, damping capacity and attenuation effects can strongly influence the received waveform. Therefore, AUWI3, AUWI4 and AUWI5 are retained as supplementary descriptors of damage-sensitive waveform behaviour, while AUWI1 and AUWI2 are treated as the more consistent indices for linear damage severity tracking within the present experimental framework.

4. Conclusions and Future Perspectives

The results presented in this study indicate that the proposed AUWI methodology successfully establishes clear correlations between acousto–ultrasonic waveform indices and impact damage severity in CFRP, FFRP and HFRP composite samples. Unlike conventional NDE techniques, which are often limited to detecting the presence and spatial extent of damage, the proposed methodology provides a quantitative basis for assessing impact damage severity. Previous approaches, such as the stress-wave factor (SWF), have shown empirical correlations with tensile strength; however, such correlations do not always provide a direct physical link with progressive damage modes, particularly when laminate layup, fibre orientation and loading direction influence the damage response.

The present study addresses these complexities by combining AUT with X-ray μCT and SEM observations. The image-based analyses confirmed that varying impact energies induced different damage modes across the investigated FRP composites. At lower impact energies, matrix cracking and early-stage delamination were more evident, whereas higher impact energies produced more severe damage modes, including extended delamination, fibre breakage, fibre pull-out and fibre–matrix debonding.

The observed correlation between AUWIs and impact energy suggests that AUWIs can effectively characterise the response of different composite materials to externally applied AU impulses. This is significant because impact energy represents an integrated measure of damage introduced into the affected material volume, while AUWIs reflect stress-wave interaction with the damaged volume between the transmitting and receiving sensors. Although a complete theoretical model directly linking each AUWI to a specific impact damage mode is not currently established, the empirical relationship between AUWIs and impact damage severity provides a practical basis for AUT-based inspection and maintenance of composite structures.

Regression analysis further confirms the effectiveness of selected AUWIs. AUWI1, corresponding to peak amplitude, and AUWI2, corresponding to wave velocity, exhibited the highest adjusted R^2 values across the tested composite samples. In particular, AUWI2 demonstrated adjusted R^2 values of approximately 0.90 ± 0.06 for CFRP, 0.88 ± 0.06 for FFRP and 0.85 ± 0.07 for HFRP composites, indicating a strong linear correlation with increasing impact severity and consistent sensitivity across different composite materials. AUWI1 also showed strong performance, with adjusted R^2 values above 0.80 in all composite material systems, supporting its role as a supplementary damage-sensitive indicator. Although AUWI3 showed reduced linearity because of energy dissipation effects, AUWI4 and AUWI5 exhibited useful responses at selected azimuthal angles, particularly for HFRP composites, indicating their potential as additional descriptors under specific material and directional conditions.

Overall, within the scope of the present linear regression-based analysis, AUWI2 demonstrated the most consistent linear association with increasing impact energy across CFRP, FFRP and HFRP composite samples. This suggests that wave velocity is a robust damage-sensitive parameter for the investigated experimental conditions. This interpretation is physically reasonable because wave velocity is influenced by the effective stiffness and continuity of the wave-propagation path, both of which are affected by matrix cracking, delamination, fibre breakage and fibre–matrix debonding. However, this conclusion should be interpreted within the limitations of the present study, as the comparison was based primarily on adjusted R^2 values obtained from individual linear regression models. No multivariate model-selection procedure, such as AIC, BIC or combined-feature classification, was applied in the present work. Therefore, AUWI2 is identified here as the most consistent single waveform index for linear damage severity tracking, rather than as an exclusive or universally superior damage indicator.

Although AUWI3, AUWI4 and AUWI5 exhibited lower adjusted R^2 values at some azimuthal angles, these indices were retained because they provide complementary physical information regarding transmitted energy, spectral redistribution and frequency-domain asymmetry. Their lower linearity indicates that they may not be suitable as standalone severity indicators across all material systems and propagation directions. However, they remain useful supplementary descriptors, particularly for complex natural and hybrid composites where attenuation, dispersion and heterogeneous fibre–matrix interactions influence the received signal.

Future work should consider multivariate statistical models, combined AUWI feature sets, machine learning classifiers and information criteria such as AIC and BIC to evaluate whether a combination of waveform indices provides stronger predictive

performance than any single AUWI. This would further improve the robustness of AUT-based damage severity assessment for composite structures under complex in-service loading conditions.

Future research should also focus on investigating the relationship between physical damage severity and the corresponding AU material response. This would improve the predictive capability of the AUWI methodology and support the development of robust tools for real-time, in-field monitoring and maintenance of advanced composite structures, including wind turbine blades, aerospace components and automotive structures.

It should also be noted that the image-based observations in the present work were primarily used to validate the dominant damage mechanisms rather than to perform full three-dimensional segmentation of crack length, delamination area or damaged volume. Future work will combine AUWI extraction with quantitative X-ray μCT image segmentation to establish direct numerical relationships between wave velocity reduction, transmitted energy loss and geometric damage descriptors such as delamination area, crack density and damaged volume fraction.

Although the present study demonstrates the potential of AUT-based waveform indices for quantifying impact damage severity in CFRP, FFRP and HFRP composite laminates, the results should be interpreted within the limitations of a controlled laboratory-scale investigation. The experiments were conducted on coupon-scale composite plates under controlled impact energies, fixed sensor spacing, controlled coupling conditions and selected azimuthal propagation directions. Therefore, the proposed methodology should be considered as a controlled validation of an AUWI-based damage severity framework rather than a fully field-deployable structural health monitoring system at this stage. The transfer of this approach to realistic wind turbine blade composites, aerospace components and other large-scale engineering structures will require further validation, because full-scale structures introduce additional complexities, including structural curvature, variable thickness, complex laminate stacking sequences, stiffeners, adhesive joints, boundary-condition effects, temperature and humidity variation, operational vibration, sensor bonding durability and in-service noise. These factors can influence stress-wave propagation, attenuation, dispersion, time-of-arrival estimation and the repeatability of AU waveform indices. Consequently, future work should validate the proposed AUWI-based framework on larger and more representative composite structures, including wind turbine blade composite subcomponents with representative curvature, thickness variation and service-like loading conditions.

Author Contributions: Conceptualisation, K.S.P.; methodology, K.S.P. and G.J.; software, K.S.P.; validation, K.S.P., G.J. and S.O.I.; formal analysis, K.S.P., G.J.; investigation, K.S.P.; resources, H.N.D.; data curation, K.S.P. and H.N.D.; writing—original draft preparation, K.S.P.; writing—review and editing, H.N.D., G.J., Y.K.C. and S.O.I.; visualisation, K.S.P.; supervision, G.J., S.O.I., Y.K.C. and H.N.D. All authors have read and agreed to the published version of the manuscript.

Funding: This research was funded by DTA3/H2020 as a part of COFUND programme with University of Hertfordshire through UK University Alliance Scheme.

Institutional Review Board Statement: Not applicable.

Informed Consent Statement: Not applicable.

Data Availability Statement: The original contributions presented in the study are included in the article, further inquiries can be directed to the corresponding authors.

Conflicts of Interest: The authors declare no conflicts of interest.

References

1. Vijayan, D.S.; Sivasuriyan, A.; Devarajan, P.; Stefańska, A.; Wodzyński, Ł.; Koda, E. Carbon Fibre-Reinforced Polymer (CFRP) Composites in Civil Engineering Application—A Comprehensive Review. *Buildings* **2023**, *13*, 1509. https://doi.org/10.3390/BUILDINGS13061509.
2. Zhi, G.; Guo, T.; Wang, J.; Chen, Z.; Wang, J. Experimental and Numerical Investigation of Machine-Induced Vibrations in Industrial Building Floors. *Eng. Struct.* **2026**, *358*, 122627. https://doi.org/10.1016/j.engstruct.2026.122627.
3. Darmon, M. Special Issue on Ultrasonic Modeling for Non-Destructive Testing. *Appl. Sci.* **2024**, *14*, 2008. https://doi.org/10.3390/APP14052008.
4. Guitard, L.; Stolidi, A.; Giakoumakis, G.; Sousa Martins, R.; Primot, J.; Jarnac, A. Robust Quantitative X-Ray Phase Diagnostic for Carbon Composite Characterisation in the Context of Lightning Induced Risk. *Sci. Rep.* **2024**, *14*, 21803. https://doi.org/10.1038/s41598-024-72087-7.
5. Gao, Y.; Hu, W.; Xin, S.; Sun, L. A Review of Applications of CT Imaging on Fiber Reinforced Composites. *J. Compos. Mater.* **2022**, *56*, 133–164. https://doi.org/10.1177/00219983211050705.
6. Garcea, S.C.; Wang, Y.; Withers, P.J. X-Ray Computed Tomography of Polymer Composites. *Compos. Sci. Technol.* **2018**, *156*, 305–319. https://doi.org/10.1016/J.COMPSCITECH.2017.10.023.
7. Azad, M.M.; Shah, A.U.R.; Prabhakar, M.N.; Kim, H.S. Deep Learning-Based Microscopic Damage Assessment of Fiber-Reinforced Polymer Composites. *Materials* **2024**, *17*, 5265. https://doi.org/10.3390/MA17215265.
8. Vary, A. The Acousto-Ultrasonic Approach. In *Acousto-Ultrasonics*; Springer: Boston, MA, USA, 1988; pp. 1–21. https://doi.org/10.1007/978-1-4757-1965-9_1.
9. Vary, A.; Bowles, K.J. An Ultrasonic-Acoustic Technique for Nondestructive Evaluation of Fiber Composite Quality. *Polym. Eng. Sci.* **1979**, *19*, 373–376. https://doi.org/10.1002/PEN.760190509.
10. Toyama, N.; Noda, J.; Okabe, T. Quantitative Damage Detection in Cross-Ply Laminates Using Lamb Wave Method. *Compos. Sci. Technol.* **2003**, *63*, 1473–1479. https://doi.org/10.1016/S0266-3538(03)00163-5.
11. Toyama, N.; Takatsubo, J. Lamb Wave Method for Quick Inspection of Impact-Induced Delamination in Composite Laminates. *Compos. Sci. Technol.* **2004**, *64*, 1293–1300. https://doi.org/10.1016/J.COMPSCITECH.2003.10.011.
12. Su, Z.; Ye, L.; Lu, Y. Guided Lamb Waves for Identification of Damage in Composite Structures: A Review. *J. Sound Vib.* **2006**, *295*, 753–780. https://doi.org/10.1016/J.JSV.2006.01.020.
13. Loutas, T.H.; Kostopoulos, V. Health Monitoring of Carbon/Carbon, Woven Reinforced Composites: Damage Assessment by Using Advanced Signal Processing Techniques. Part II: Acousto–Ultrasonics Monitoring of Damage Development. *Compos. Sci. Technol.* **2009**, *69*, 273–283. https://doi.org/10.1016/J.COMPSCITECH.2008.09.042.
14. De Luca, A.; Caputo, F.; Sharif Khodaei, Z.; Aliabadi, M.H. Damage Characterization of Composite Plates under Low Velocity Impact Using Ultrasonic Guided Waves. *Compos. B Eng.* **2018**, *138*, 168–180. https://doi.org/10.1016/J.COMPOSITESB.2017.11.042.
15. Hervin, F.; Maio, L.; Fromme, P. Guided Wave Scattering at a Delamination in a Quasi-Isotropic Composite Laminate: Experiment and Simulation. *Compos. Struct.* **2021**, *275*, 114406. https://doi.org/10.1016/J.COMPSTRUCT.2021.114406.
16. Elanchezhian, C.; Ramnath, B.V.; Hemalatha, J. Mechanical Behaviour of Glass and Carbon Fibre Reinforced Composites at Varying Strain Rates and Temperatures. *Procedia Mater. Sci.* **2014**, *6*, 1405–1418. https://doi.org/10.1016/j.mspro.2014.07.120.
17. Vary, A.; Lark, R.F. Correlation of Fiber Composite Tensile Strength with the Ultrasonic Stress Wave Factor. *J. Test. Eval.* **1979**, *7*, 185–191. https://doi.org/10.1520/JTE11379J.
18. *ASTM D2344/D2344M-22*; Standard Test Method for Short-Beam Strength of Polymer Matrix Composite Materials and Their Laminates. ASTM International: West Conshohocken, PA, USA, 2022.
19. Ricci, F.; Monaco, E.; Boffa, N.D.; Maio, L.; Memmolo, V. Guided Waves for Structural Health Monitoring in Composites: A Review and Implementation Strategies. *Prog. Aerosp. Sci.* **2022**, *129*, 100790. https://doi.org/10.1016/J.PAEROSCI.2021.100790.
20. Tanveer, M.; Elahi, M.U.; Jung, J.; Azad, M.M.; Khalid, S.; Kim, H.S. Recent Advancements in Guided Ultrasonic Waves for Structural Health Monitoring of Composite Structures. *Appl. Sci.* **2024**, 14, 11091. https://doi.org/10.3390/APP142311091.
21. Katunin, A.; Wronkowicz-Katunin, A.; Danek, W.; Wyleżoł, M. Modeling of a Realistic Barely Visible Impact Damage in Composite Structures Based on NDT Techniques and Numerical Simulations. *Compos. Struct.* **2021**, *267*, 113889. https://doi.org/10.1016/J.COMPSTRUCT.2021.113889.
22. Tabatabaeian, A.; Jerkovic, B.; Harrison, P.; Marchiori, E.; Fotouhi, M. Barely Visible Impact Damage Detection in Composite Structures Using Deep Learning Networks with Varying Complexities. *Compos. B Eng.* **2023**, *264*, 110907. https://doi.org/10.1016/J.COMPOSITESB.2023.110907.

23. Hervin, F.; Fromme, P. Anisotropy Influence on Guided Wave Scattering for Composite Structure Monitoring. *Struct. Health Monit.* **2023**, *22*, 2626–2640. https://doi.org/10.1177/14759217221133284.
24. Azad, M.M.; Munyaneza, O.; Jung, J.; Sohn, J.W.; Han, J.W.; Kim, H.S. Damage Localization and Severity Assessment in Composite Structures Using Deep Learning Based on Lamb Waves. *Sensors* **2024**, *24*, 8057. https://doi.org/10.3390/S24248057.
25. Andersen, K.G.; Jombo, G.; Ismail, S.O.; Chen, Y.K.; Dhakal, N.; Zhang, Y.; Andersen, K.G.; Jombo, G.; Ismail, S.O.; Chen, Y.K.; et al. Damage Characterisation in Composite Laminates Using Vibro-Acoustic Technique. In *Energy and Sustainable Futures: Proceedings of 2nd ICESF 2020*; Springer International Publishing: Cham, Switzerland, 2021; pp. 275–282. https://doi.org/10.1007/978-3-030-63916-7_34.
26. Kiernan, M.T. A Physical Model for the Acousto-Ultrasonic Method. Virginia Polytechnic Institute and State University, Blacksburg, VA, USA, 1989.
27. Kiernan; Duke, P.C. Analysis of an Acousto-Ultrasonic Signal | Semantic Scholar. Available online: https://www.semanticscholar.org/paper/PC-analysis-of-an-acousto-ultrasonic-signal-Kiernan-Duke/77a349f8e0a823ef45cf747e89c961e583ddf223 (accessed on 20 July 2022).
28. Vary, A. Acousto-Ultrasonics Approach. *Natl. Aeronaut. Space Adm.* **1988**, *2*, 1–54.
29. Talreja, R. *Fatigue of Composite Materials*; Technomic Publishing: Lancaster, PA, USA, 1987.
30. Draper, N.R.; Smith, H. *Applied Regression Analysis*; John Wiley & Sons: Hoboken, NJ, USA, 2014; pp. 1–716. https://doi.org/10.1002/9781118625590.
31. Montgomery, D.C.; Peck, E.A.; Vining, G.G. *Introduction to Linear Regression Analysis*, 5th ed.; Wiley: Hoboken, NJ, USA, 2012. Available online: https://www.scirp.org/reference/referencespapers?referenceid=2191029 (accessed on 25 May 2026).
32. Akaike, H. A New Look at the Statistical Model Identification. *IEEE Trans. Automat. Contr.* **1974**, *19*, 716–723. https://doi.org/10.1109/TAC.1974.1100705.
33. Schwarz, G. Estimating the Dimension of a Model. *Ann. Stat.* **1978**, *6*, 461–464. https://doi.org/10.1214/AOS/1176344136.
34. Basri, R.; Chiu, W.K. Numerical Analysis on the Interaction of Guided Lamb Waves with a Local Elastic Stiffness Reduction in Quasi-Isotropic Composite Plate Structures. *Compos. Struct.* **2004**, *66*, 87–99. https://doi.org/10.1016/J.COMPSTRUCT.2004.04.025.
35. Dhakal, H.N.; Zhang, Z.Y.; Bennett, N.; Reis, P.N.B. Low-Velocity Impact Response of Non-Woven Hemp Fibre Reinforced Unsaturated Polyester Composites: Influence of Impactor Geometry and Impact Velocity. *Compos. Struct.* **2012**, *94*, 2756–2763. https://doi.org/10.1016/J.COMPSTRUCT.2012.04.004.
36. Yarlagadda, S.; Lesieutre, G. Fiber Contribution to Modal Damping of Polymer Matrix Composite Panels. *J. Spacecr. Rocket.* **2012**, *32*, 825–831. https://doi.org/10.2514/3.26691.
37. Daoud, H.; Rebière, J.L.; Makni, A.; Taktak, M.; El Mahi, A.; Haddar, M. Numerical and Experimental Characterization of the Dynamic Properties of Flax Fiber Reinforced Composites. *Int. J. Appl. Mech.* **2016**, *8*, 1650068. https://doi.org/10.1142/S175882511650068X.